

Reducing quantum resources for observable estimation with window-assisted coherent QPE

Harriet Apel^{1,2}, Cristian L. Cortes¹, Jessica Lemieux¹, Mark Steudtner¹

¹*PsiQuantum, 700 Hansen Way, Palo Alto, CA 94304, USA* ²*Department of Computer Science, UCL, Gower Street, London, UK*

Abstract

Quantum Phase Estimation (QPE) routines are known to fail probabilistically even with perfect gates and input states. This effect stems from an incompatibility of finite-sized quantum registers to capture a phase within QPE with phase angles of infinite precision, and the effect extends even beyond what would be reasonably expected from rounding. This effect can be partially mitigated by biasing the phase register with a window, or taper state, from classical signal processing. This paper focuses on how windowing a *coherent* QPE used as a subroutine can improve the accuracy of the overall algorithm. Specifically we study the quantum task of estimating observables where window-assisted coherent QPE is used as a subroutine to implement a reflection about an eigenstate. Quantum resource estimates show over 2-orders-of-magnitude reduction in Toffoli counts over the previous costed techniques – also assisted by the use of improved block encoding techniques – demonstrating an encouraging decrease in resources for quantum computation of molecular observables. Since QPE, as one of only a few quantum building blocks, appears as a subroutine in many algorithms; this analysis also provides a model for understanding how window functions propagate to an improved error in composite algorithms.

Quantum phase estimation (QPE) is a seminal routine in quantum algorithms, leveraging the quantum Fourier transform (QFT) to learn the eigenphase of a unitary with respect to a particular eigenstate. In addition to the qubits required to describe the system, the routine requires a phase register that is measured to extract the eigenphase. In practice, the phase register consists of a finite number of qubits and introduces a ‘bit discretisation’ effect. This does not only result in the coarsening of data into bins of finite precision, but distorts the probability distribution of the measured phase state. Therefore, even given an exact eigenstate as input, with non-zero probability the final phase register measurement obtains an outcome far from the true eigenphase – this failure probability can be as high as 19%. This affects the success probability of the routine, necessitating repetitions to learn the phase with confidence. Bit discretisation can be well understood from the vantage of classical signal processing, as this distortion has the same origins as performing a Fourier transform on a time-limited signal [39].

It was also noted that preparing the register that holds the phase estimate in a superposition with non-uniform amplitudes can reduce the effect of bit discretisation. A uniform superposition is akin to sampling the signal from a rectangular window with sharp discontinuities at the periodic boundary, whereas a tapered window function dampens these discontinuity and reduces the distortion of the probability distribution. While being ubiquitous in classical signal processing, window functions have been used in quantum both to asymptotically reduce query counts [4, 2] and to practically outperform quantum signal processing (QSP) in small instances [16].

There are two important quantities to assess the utility of an algorithm: the *success probability* describing the likelihood that a given run of the algorithm produces a “correct result”; and the *error* describing the maximum deviation from the true value that we are willing to accept as a “correct result”. For example, if the true value is x_0 , we allow an error of ϵ and the algorithm produces the result x according to some distribution, then the success probability of the algorithm is $P(|x - x_0| \leq \epsilon)$.

In standalone QPE – where the phase register is directly measured – window functions can increase the success probability of the algorithm for a given error but increasing the accuracy can only be improved by increasing the number of phase qubits to achieve a lower error. This work studies window functions for *coherent* QPE subroutines within a larger algorithm. The coherent nature of the QPE indicates that the phase register is not measured at the end of the routine and instead further gates are applied using the full phase register state for computation. Therefore, instead of a failure probability, we consider a failure amplitude of the subspace spanned by $\{|x\rangle\}$ with $|x - x_0| > \epsilon$. This introduces a mid-circuit error, hence improving the success amplitude using window functions in coherent QPE increases the accuracy of the overall algorithm and can help achieve a lower error tolerance. Improving the algorithmic error is more compelling than improving the success probability, since while the latter can be compensated by taking repeated measurements, improving the former requires resources such as additional gates and logical qubits which will determine whether such algorithms can be run on limited hardware at all.

A notable application of coherent QPE is in estimating the expectation value of an operator with respect to a system’s ground state [24, 33, 40]. This is an interesting case study since the concatenated nature of the algorithm nicely demonstrates the propagation from the QPE success amplitude to the overall algorithmic error. Furthermore, it is one of the few fault-tolerant algorithms using a coherent QPE where the quantum resources have been numerically estimated [40]. The natural context for this algorithm is the estimation of quantum observables on ground states of molecular systems, which has profound applications in computational chemistry. Expectation values of unperturbed wavefunctions may be used to estimate first-order molecular properties such as molecular multipole moments, forces on nuclei and stationary points on potential energy surfaces [14, 10]. Furthermore, they can also be used to compute higher-order properties such as polarizability and harmonic vibrational frequencies with additional post-processing [20]. These properties play a significant role in predicting reactivity and as well as understanding spectroscopic data. The finite phase register in the QPE subroutine introduces a bit discretisation that degrades the algorithmic error – reducing the precision to which we can learn these molecular properties.

This work both analyses the error of this algorithm when the QPE phase register is unitarily prepared in a general state and demonstrates the practical benefit of choosing the Kaiser window [23] as the phase register taper function. The error analysis demonstrates that coherent use of QPE is exactly where introducing window functions can have the most significant reduction in quantum resources. As is somewhat expected due to the complex nature of the question, our resource estimates still clearly place this algorithm in the regime requiring a large-scale fault-tolerant quantum computer. However, the advantage of using window functions over other techniques to combat bit discretisation in QPE (such as applying QSP to round phase values in QPE [36]) is seen via order-of-magnitude reductions in the number of Toffoli gates required to estimate molecular observables. We also show that this reduction is further improved by using state of the art block-encoding methods [37, 26, 12] as well as adapting recent tensor factorisation methods (BLISS-THC) to simultaneously optimise the Hamiltonian and observable rank truncation parameters.

The technical background of both window-assisted QPE and the expectation value algorithm is first given in Section 1. Slight modifications to previous expectation value algorithms [24, 33, 40] are required to capture the benefit of window-assisted QPE, so this is presented and analysed in Section 2. Finally the numerical evidence of window functions reducing quantum resources is attested in Section 3 where the Toffoli and qubit counts are compared with the state of the art.

1 Technical background

1.1 QPE with window functions

Given controlled access to a unitary U , along with copies of an eigenstate $|\psi\rangle$, the goal of QPE is to estimate the eigenphase $\phi \in [0, 1]$: $U|\psi\rangle = e^{2\pi i \phi}|\psi\rangle$. More generally, given copies of any

state $|\nu\rangle = \sum_i c_i |\psi_i\rangle$ written here in the eigenbasis of U , measuring the phase qubits of a QPE probabilistically projects the state onto an eigenstate $|\psi_i\rangle$ and estimates the corresponding eigenphase ϕ_i . To introduce window functions, we initially assume exact copies of an eigenstate $|\psi\rangle$ for simplicity. QPE requires a quantum register for the system that supports the input state $|\psi\rangle$ (denoted ‘‘sys’’), and an additional n qubit quantum register to extract the phase (denoted ‘‘ph’’). This phase register is unitarily prepared in some superposition over the computational basis states, $\hat{W}|a\rangle_{\text{ph}} = \sum_{x=0}^{2^n-1} W_a(x)|x\rangle_{\text{ph}}$. Given that the phase register is initially prepared in $|0\rangle_{\text{ph}}$ the total input state for the QPE is $|\psi\rangle_{\text{sys}} \otimes \sum_{x=0}^{2^n-1} W_0(x)|x\rangle_{\text{ph}}$. The typical choice for this function is the rectangular window $W_0(x) = \sqrt{1/2^n}$, efficiently prepared by applying parallel Hadamard gates $\hat{W} = H^{\otimes n}$. Controlled U ’s are then applied to kickback the eigenphase of $|\psi\rangle$ onto the phase register. Finally, an inverse quantum Fourier transform and then measurement of the phase register allows an estimate of the eigenphase to be obtained. Given the eigenbasis for the Hamiltonian is $\{|\psi_i\rangle\}$ with corresponding eigenphases $\{\phi_i\}$ the unitary action of QPE is given by

$$\text{QPE} = \sum_{i=0}^{2^t-1} |\psi_i\rangle\langle\psi_i|_{\text{sys}} \otimes \sqrt{\frac{1}{2^n} \sum_{a,k=0}^{2^n-1} \left(\sum_{x=0}^{2^n-1} W_a(x) e^{2\pi i (2^n \phi_i - k) \frac{x}{2^n}} \right)} |k\rangle\langle a|_{\text{ph}}. \quad (1)$$

Consider the state $\text{QPE}|\psi_i\rangle_{\text{sys}}|0\rangle_{\text{ph}}$ where the rectangular window is used in the QPE, the squared amplitude of the phase register in the k^{th} computational basis state is given by

$$P_k = \left| \frac{1}{2^n} \sum_{x=0}^{2^n-1} e^{2\pi i (2^n \phi_i - k) \frac{x}{2^n}} \right|^2. \quad (2)$$

If ϕ_i is exactly representable by n bits (i.e. $2^n \phi_i \in \mathbb{Z}^+$) then algorithmically the if measured eigenphase is obtained exactly with certainty, i.e. $P_{k=2^n \phi_i} = 1$. However, as generally this is not the case ($2^n \phi_i$ is non-integer) bit discretisation is introduced. If one were to directly measure the phase register the outcomes are sampled from a probability distribution, requiring repeated runs of the QPE circuit to learn the histogram. The number of phase qubits can be increased to improve the error and the success probability of the algorithm. To learn ϕ_i to precision ϵ with probability $(1 - \delta)$ requires $n \in O(\log \frac{1}{\epsilon})$ qubits and $O\left(\frac{\log(1/\delta)}{\epsilon}\right)$ calls to controlled U [29].

It is insightful to analyse QPE through the lens of Fourier analysis. Inside the modulus of the right-hand side of Eq. (2) is the discrete Fourier transform (DFT) of an oscillating function with frequency ϕ . The window function modulates the oscillation $e^{2\pi i \phi x} \mapsto W_a(x)e^{2\pi i \phi x}$ before the DFT. In the resulting probability distribution, the frequency domain of the window function is convoluted with the delta peak $\delta_{k, 2\pi\phi}$. This convolution distorts the distribution giving rise to non-zero amplitude to $|k\rangle$ where k is far from $2\pi\phi$. The rectangular window, due to the large sidebands of the sinc function, has particularly problematic distortion.

This viewpoint of Fourier analysis links the problem of *bit discretisation* in QPE to the problem of *spectral leakage* in classical signal processing, a well-studied problem [9, 19]. One solution from signal processing is to replace the rectangular window function to reduce this effect. Given a time-limited function, instead of using the discontinuous rectangle function, the envelope is tapered to ‘smooth out’ the edges. This is helpful since the FT of a tapered function has less amplitude in side-bands than the sinc function [23] and therefore can lead to less distortion. See Fig. 1 for an illustration. This idea can be applied to QPE by preparing the phase register, not in an equal superposition, but with some non-uniform window function with tapered amplitudes [39]. These amplitudes carry through the circuit so the squared amplitude of $|k\rangle_{\text{ph}}$ is now more generally:

$$P_k = \left| \sqrt{\frac{1}{2^n} \sum_{x=0}^{2^n-1} W_0(x) e^{2\pi i (2^n \phi - k) \frac{x}{2^n}}} \right|^2. \quad (3)$$

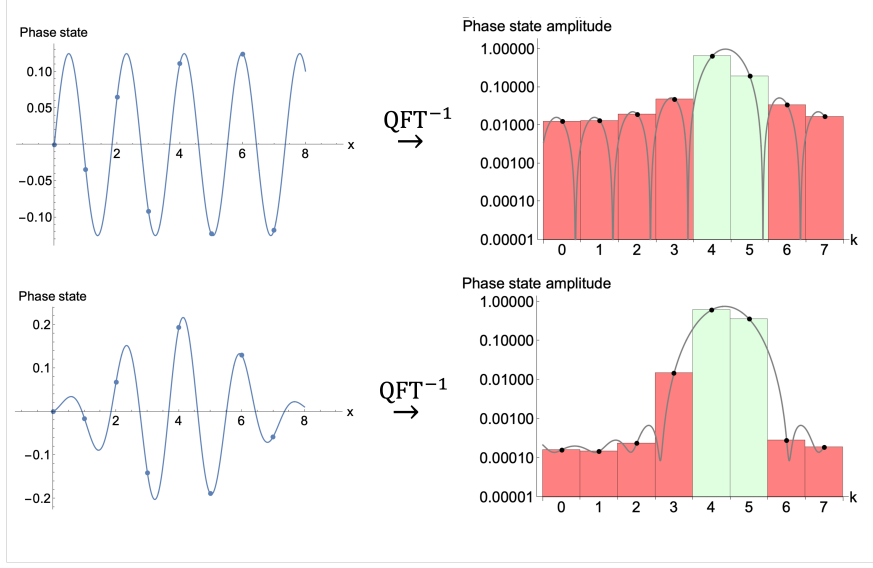


Figure 1: Bit discretisation and the link to classical signal processing. **Top:** An oscillation function is multiplied by a rectangular function, the frequency is such that the signal is not periodic and therefore $2\pi\phi$ is non-integer. After the inverse QFT the phase state amplitude distribution is given by a sinc function centered at $2\pi\phi$. When sampled, due to the *side bands* of the sinc function, there is some amplitude in bins that are far from the true frequency – shown in pink. Note that if $2\pi\phi$ was an integer the distortion of the function is hidden by sampling the zeros of the sinc, recovering the original delta function. **Bottom:** Now instead of a rectangular window a smooth envelop function modulates the oscillation from above. After the inverse QFT the amplitude is more concentrated in the two bins closest to the true phase – shown in green as the *central lobe* – due to the smaller side bands of window Fourier transform.

Many different window functions exist, one good candidate is the Kaiser function [23]:

$$K(x, \beta) = \sqrt{\frac{1}{\mathcal{N}} \frac{I_0(\beta\sqrt{1-\bar{x}^2})}{I_0(\beta)}}, \quad (4)$$

where I_0 is the 0th order modified Bessel function and \mathcal{N} is a normalisation constant. To use this window function the phase register is prepared in the Kaiser state: $\hat{W}|0\rangle_{\text{ph}} = \sum_{x=0}^{2^n-1} K(x, \beta)|x\rangle_{\text{ph}}$. The Kaiser window is tractable to analysis – it has been shown to reduce the query complexity of QPE with error ϵ and success probability $(1-\delta)$ to $O(\epsilon^{-1} \log(\delta^{-1}))$ [4] – an exponential improvement in δ . The window is tunable with the bandwidth parameter, β . Larger β corresponds to a narrower distribution and therefore a Fourier transform with wider bandwidth and lower amplitude in sidebands.

The exponentially improved complexity of QPE with the Kaiser window has been used to analyse more complex quantum algorithms [2, 4, 5]. However, there has been little work considering the non-asymptotic advantage of using windowed QPE in a coherent setting to combat bit discretisation over other more involved rounding techniques such as QSP.

Coherent QPE for reflections

QPE can also be a useful subroutine within a more complex algorithm. Here it is performed coherently and failure amplitude in the phase register is fed through to subsequent gates and contributes to a mid-circuit error. Therefore, instead of manifesting as a failure probability, in coherent QPE the finite size effects of the phase register propagates to an algorithmic error.

QPE can be used coherently to approximately implement a reflection about an eigenstate $R_{\psi_0} = \mathbb{1} - 2|\psi_0\rangle\langle\psi_0|$ within a subspace, given a t -qubit unitary U such that $|\psi_0\rangle$ is an eigenstate with eigenphase ϕ_0 . QPE acts jointly on this system register of t qubits and an ancillary phase register of n qubits. To implement an approximate reflection about a state using QPE, the n -bit approximation of the eigenphase (denoted $\tilde{\phi}_0$) must be known in advance. The circuit for the reflection then consists of a QPE of U , a phase register reflection about $|\tilde{\phi}_0\rangle_{\text{ph}}$ and finally uncomputing the QPE: $R_{\psi_0} \approx \text{QPE}^\dagger(\mathbb{1} - 2|\tilde{\phi}_0\rangle\langle\tilde{\phi}_0|_{\text{ph}})\text{QPE}$. This can be less resource intensive than a direct implementation using QSP which requires precisely computing many phase factors [15, 18, 13].

Inaccuracy in phase estimation now leads to implementing a distorted unitary reflecting about some contaminated state. Instead of reflecting a single eigenstate $|\phi_0\rangle$ the reflection occurs about a perturbed state with non-zero amplitude in other eigenstates. Unless *all* eigenphases are exactly representable in n bits, the reflection unitary will be perturbed. The QPE based reflection takes the form:

$$\begin{aligned} \text{QPE}^\dagger(\mathbb{1} - 2|\tilde{\phi}_0\rangle\langle\tilde{\phi}_0|_{\text{ph}})\text{QPE} &= \mathbb{1} - 2 \sum_{i=0}^{2^t-1} |\psi_i\rangle\langle\psi_i|_{\text{sys}} \otimes \\ &\quad \frac{1}{2^n} \sum_{a,a'=0}^{2^n-1} \left(\sum_{x=0}^{2^n-1} W_a(x) e^{2\pi i(\phi_i - \tilde{\phi}_0)x} \right) \left(\sum_{x'=0}^{2^n-1} W_{a'}^*(x') e^{-2\pi i(\phi_i - \tilde{\phi}_0)x'} \right) |a'\rangle\langle a|_{\text{ph}}. \end{aligned} \quad (5)$$

Using an appropriate window function can bring this operation closer to the intended reflection about $|\psi_0\rangle_{\text{sys}} \otimes |0\rangle_{\text{ph}}$.

1.2 Expectation value algorithms

One of the attractive future applications of quantum computers is to improve speed and accuracy of *in silico* quantum chemistry simulations. Aside from molecular ground state energy estimation, a task with promising quantum advantage is estimating other molecular observables with respect to a state of interest. Algorithmically the goal is to estimate $\langle\sigma_0|\hat{F}|\sigma_0\rangle$: the expectation value of some observable \hat{F} with respect to the ground state, $|\sigma_0\rangle$, of a Hamiltonian, H . Moreover, generally the Hamiltonian does not commute with \hat{F} .

The approach of repeatedly preparing the state $|\sigma_0\rangle$ to measure the expectation value requires $O(\epsilon^{-2})$ queries to a block encoded Hamiltonian. This was improved in [24, 35, 33, 40] to $O(\epsilon^{-1})$ by instead performing amplitude estimation [7] of some walk operator¹. This work leverages the walk operator from [33, 40] $\mathcal{U} := (\mathcal{B}[\hat{F}]) \cdot (c\text{-}R_{\sigma_0})$, the product of $\mathcal{B}[\hat{F}]$ a *self-inverse* block encoding of the non-unitary observable and $c\text{-}R_{\sigma_0}$ a controlled reflection about $|\sigma_0\rangle$. The block encoding of the observable \hat{F} necessitates an ancillary quantum register we label \mathcal{B}_F . The reflection about the state is then controlled on $|0\rangle_{\mathcal{B}_F}$ to select for the encoding subspace.

Definition 1 (Block encoding). *Consider the Hermitian operator \hat{F} acting on \mathcal{H}_{sys} . A *self-inverse* block encoding of the operator $\mathcal{B}[\hat{F}]$ is a unitary operator acting on $\mathcal{H}_{\text{sys}} \otimes \mathcal{H}_{\mathcal{B}_F}$ that encodes \hat{F} in a subspace $(|0\rangle_{\mathcal{B}_F} \otimes \mathbb{1}_{\text{sys}}) \mathcal{B}[\hat{F}] (|0\rangle_{\mathcal{B}_F} \otimes \mathbb{1}_{\text{sys}}) = \hat{F}$.*

The algorithm hinges on a relation between the eigenphase of the walk operator \mathcal{U} and the desired expectation value $\langle\sigma_0|\hat{F}|\sigma_0\rangle$. This can be understood via a general result about the product of two reflections:

Lemma 1. [[42] or [31, Appendix A]] *Consider two reflections:*

$$R_A = \mathbb{1} - 2\Pi_A \quad \text{and} \quad R_B = \mathbb{1} - 2\Pi_B,$$

¹There is also work considering the complexity of estimating M observables. [22] show that the $O(\epsilon^{-1})$ scaling in the worst case comes at a cost of linear complexity in the number of observables. Shadow estimation protocols [1] obtain a $O(\log(M))$ scaling at the price of a poor accuracy scaling $O(\epsilon^{-4})$. This can be improved to $\tilde{O}(\epsilon^{-2})$ by using randomised shadow estimation circuits [21] but only for restricted observables that do not introduce a scaling of the system Hilbert space into the complexity.

where ω_k are the singular values of the projector product $\Pi_A \cdot \Pi_B$. The product of these reflections $\mathcal{U} := R_B R_A$ is a unitary with eigenphases:

$$\theta_{k,\pm} = \mp \frac{1}{2\pi} \cos^{-1} \left(2|\omega_k|^2 - 1 \right).$$

While a known result, the proof of Lemma 1 is given in Appendix A for completeness. The connection made in [24, 33, 40] between phase estimation of the walk operator and expectation value estimation is manifest when considering the reflections² $\mathcal{B}[\hat{F}]$ and $c - R_{\sigma_0}$ with the above result.

Theorem 2. Consider the walk operator $\mathcal{U} := (\mathcal{B}[\hat{F}]) \cdot (c - R_{\sigma_0})$ acting on $\mathcal{H}_{\text{sys}} \otimes \mathcal{H}_{\mathcal{B}_F}$ where $\mathcal{B}[\hat{F}]$ is a self-inverse block encoding of the renormalised observable \hat{F} ($\|\hat{F}\|_{\text{op}} \leq 1$) and $c - R_{\sigma_0}$ is the reflection about a groundstate, $|\sigma_0\rangle_{\text{sys}}$, controlled on the $|0\rangle_{\mathcal{B}_F}$ subspace. The state $|\sigma_0\rangle_{\text{sys}} \otimes |0\rangle_{\mathcal{B}_F}$ is an equal superposition of two eigenstates of \mathcal{U} with eigenphases,

$$\theta_{0,\pm} = \mp \frac{1}{2\pi} \cos^{-1} \left(\langle \sigma_0 | \hat{F} | \sigma_0 \rangle \right).$$

Theorem 2 simply applies Lemma 1 to two particular reflections – see e.g. [40] for further details of this result or Appendix A for a proof given for self-containment. Since $\theta_{0,\pm}$ is a simple function of the desired expectation value, $\langle \sigma_0 | \hat{F} | \sigma_0 \rangle$ can be calculated from an estimate of this eigenphase.

QPE in expectation value algorithms

In the quantum algorithm to estimate $\langle \sigma_0 | \hat{F} | \sigma_0 \rangle$ there are two potential subroutines where QPE can be used. QPE of the walk operator is used incoherently to estimate the eigenphase $\theta_{0\pm}$, called the outer QPE or oQPE. Additionally, QPE can be used coherently to implement the reflection about a state needed to construct the walk operator, called the inner QPE or iQPE. The first non-asymptotic resource estimates for this routine were given in [40] where the reflection about the state is instead constructed via phase estimation due to the challenging classical pre-processing requirements of using QSP. Both types of QPE will have finite phase registers which we will denote by Hilbert spaces \mathcal{H}_{iph} (\mathcal{H}_{oph}) for the inner (outer) QPE. These will both introduce bit discretisation and degrade the performance of the algorithm.

Eq. (5) described how QPE can be used to reflect about an eigenstate of a unitary, however $|\sigma_0\rangle$ is an eigenstate of the non-unitary Hamiltonian. Therefore, the iQPE will reflect about the eigenstate of the qubitised encoding of the Hamiltonian, $\mathcal{Q}[H]$, acting jointly on $\mathcal{H}_{\text{sys}} \otimes \mathcal{H}_{\mathcal{B}_H}$. This encoding is simply related to the self-inverse block encoding (denoted $\mathcal{B}[\cdot]$) by a reflection,

$$\mathcal{Q}[H] := (2|0\rangle\langle 0| - \mathbb{1})_{\mathcal{B}_H} \otimes \mathbb{1}_{\text{sys}} \cdot \mathcal{B}[H] \quad (6)$$

and therefore still encodes the operator in a subspace, $((0|_{\mathcal{B}_H} \otimes \mathbb{1}_{\text{sys}}) \mathcal{Q}[H] (|0\rangle_{\mathcal{B}_H} \otimes \mathbb{1}_{\text{sys}})) = H$. However, instead of being self-inverse the qubitised encoding has eigenphases related to the eigenvalues of the encoded operator [27]. If the Hamiltonian has eigenvectors $\{|\sigma_i\rangle\}_{i=1}^t$ with eigenvalues $\{\lambda_i\}_{i=1}^t$ then the qubitised Hamiltonian encoding has eigenvectors,

$$\{|\psi_{i,\pm}\rangle := \frac{1}{\sqrt{2}} \left(\mathbb{1} \pm i \frac{\lambda_i \mathbb{1} - \mathcal{Q}[H]}{\sqrt{1 - \lambda_i}} \right) |\sigma_i\rangle_{\text{sys}} \otimes |0\rangle_{\mathcal{B}_H} \}, \quad (7)$$

with eigenphases $\{\phi_{i,\pm} := \pm \frac{1}{2\pi} \cos^{-1}(\lambda_i)\}$.

² $\mathcal{B}[\hat{F}]$ is also a reflection due to being self-inverse and so Lemma 1 can be applied.

2 Algorithm analysis

Recall that ideally the expectation algorithm uses the coherent iQPE to implement a reflection about the qubitised Hamiltonian groundstate,³ $|\psi_{0,+}\rangle_{\text{sys},\mathcal{B}_H}$. However, a finite iQPE phase register only approximately achieves this, instead implementing

$$R_{\tilde{\psi}_{0,+}} := \text{QPE}^\dagger(\mathbb{1} - 2|\tilde{\phi}_{0,+}\rangle\langle\tilde{\phi}_{0,+}|)_{\text{iph}}\text{QPE}. \quad (8)$$

Note that since the circuit includes a reflection about $|\tilde{\phi}_{0,+}\rangle_{\text{iph}}$ the eigenphase must be learned precisely. Since $(R_{\tilde{\psi}_{0,\pm}})^2 = \mathbb{1}$, regardless of the accuracy of the iQPE, and whether techniques such as QSP or window functions are used, the implementation is still a true reflection. Therefore, while not immediate from Eq. (5), there exists a projector \tilde{P} such that $R_{\tilde{\psi}_{0,+}} = \mathbb{1} - 2\tilde{P}$. The block encoding of the observable \hat{F} is self-inverse and therefore is the second reflection, with an associated projector $Q := \frac{1}{2}(\mathbb{1} - \mathcal{B}[\hat{F}])$. Therefore Lemma 1 can be used to analyse the spectra of the resulting walk operator via the squared projector product, $\tilde{P} \cdot Q \cdot \tilde{P}$, despite the approximate implementation.

In standalone QPE – where the goal is to estimate the eigenphase of a given eigenstate – window functions improve the *success probability* of the algorithm but leave the accuracy unchanged. In contrast, due to the concatenated nature of using QPE as a subroutine, improving the success probability of the iQPE can lead to *increased accuracy* of the oQPE. Finite register effects in the iQPE perturbs the reflection and affects the eigenspectra of $\tilde{P} \cdot Q \cdot \tilde{P}$ and hence \mathcal{U} . Perturbation of the eigenphase of \mathcal{U} translates into *error* in the expectation value estimate whereas perturbation of the eigenvectors lead to decreased success probability of the oQPE.

The expectation value circuit proposed here (see Fig. 2a) has two key distinctions from previous work, to leverage window-assisted QPE as a subroutine. Firstly, the phase register is prepared with a state preparation circuit, this is more costly than simply applying Hadamards. Secondly the observable block encoding is controlled on the phase register, introducing additional interplay between the reflections so that the preparation unitaries do not commute through the circuit and cancel. Both these distinctions add complexity into each query to \mathcal{U} . However, we will show that this is offset by the gain of implementing a \mathcal{U} closer to the idealised state reflection. Numerically this overall leads to trimmed gate counts for observable estimation.

2.1 Effect of window functions on the walk operator

By preparing the iQPE phase register with a unitary \hat{W} , window functions improve the accuracy of the reflection implementation for general QPE unitaries. The projector is expressed in terms of the window function,

$$\tilde{P} = \sum_{i=0}^{2^t-1} \sum_{\{\pm\}} |\psi_{i,\pm}\rangle\langle\psi_{i,\pm}|_{\text{sys},\mathcal{B}_H} \otimes \frac{1}{2^n} \sum_{a,a',x,x'=0}^{2^n-1} W_a(x) W_{a'}^*(x') e^{2\pi i(\phi_{i,\pm} - \tilde{\phi}_{0,+})(x-x')} |a'\rangle\langle a|_{\text{iph}}. \quad (9)$$

Let us define the useful phase register state

$$|\rho(y)\rangle_{\text{iph}} := \frac{1}{\sqrt{2^n}} \sum_{a,x=0}^{2^n-1} W_a^*(x) e^{-2\pi i y x / 2^n} |a\rangle_{\text{iph}}. \quad (10)$$

Physically this is the phase register state initially in $|a\rangle_{\text{iph}}$ after the circuit for R_ψ has been applied. The value of y then depends on the relative difference between the reflection phase and the phase applied by the QPE, $(\phi_{j,\pm} - \tilde{\phi}_{0,+})$, where recall that $\tilde{\phi}_{0,+}$ is the closest n -bit representation of $\phi_{0,+}$. Since

³Here we have arbitrarily selected the positive block encoding branch. This introduces a factor of $\sqrt{1/2}$ in the success amplitude.

we are concerned with the qubitised Hamiltonian eigenbasis for the system, for convenience introduce the abbreviated notation $|\rho_i^\pm\rangle := |\rho(\phi_{j,\pm} - \tilde{\phi}_{0,+})\rangle$. The projector associated with the reflection can then be rewritten more succinctly as,

$$\tilde{P} = \sum_{i=0}^{2^t-1} \sum_{\{\pm\}} |\psi_{i,\pm}\rangle\langle\psi_{i,\pm}|_{\text{sys},\mathcal{B}_H} \otimes |\rho_i^\pm\rangle\langle\rho_i^\pm|_{\text{iph}}. \quad (11)$$

We can now outline the expectation value algorithm – note that before executing the algorithm, it is necessary to have a good approximation of the ground state energy, an estimate of the spectral gap, and a means of preparing the ground state.

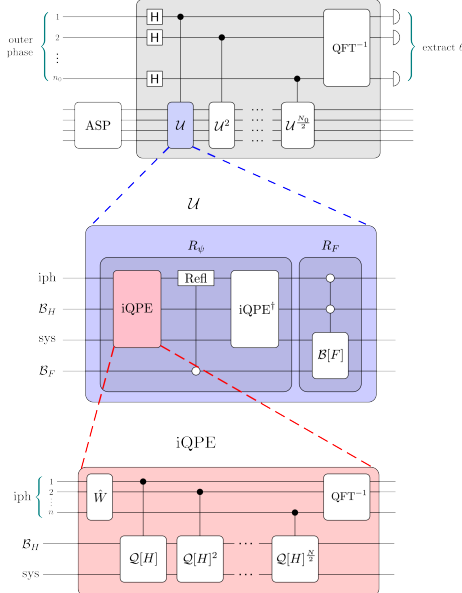


Figure 2(a): Circuit for Algorithm 1.

Algorithm 1. *Expectation value estimation: estimate $\langle\psi_0|\hat{F}|\psi_0\rangle$ to within ϵ with success probability p_{success}*

1. Prepare the state $|\psi_{0,+}\rangle_{\text{sys},\mathcal{B}_H} \otimes |0\rangle_{\mathcal{B}_F}$ using any arbitrary state preparation routine (ASP).
2. Run the circuit, replacing R_F by $\mathbb{1} - 2|00\rangle\langle 00|_{\mathcal{B}_H,\mathcal{B}_F}$ in \mathcal{U} to estimate $\theta'_{0,\pm} = \pm \frac{1}{\pi} \cos^{-1}(2|\langle\rho_0^+|0\rangle|^2 - 1)$
3. Classical processing: from $\theta'_{0,\pm}$ calculate the overlap $|\langle\rho_0^+|0\rangle|$
4. Run the circuit using the observable \hat{F} to estimate $\theta_{0,\pm}$ from Lemma 3
5. Classical processing: from $\theta_{0,\pm}$ calculate $\langle\sigma_0|\hat{F}|\sigma_0\rangle$ up to error ϵ (Proposition 5)

An understanding of the eigenspectra of \mathcal{U} , when window-assisted iQPE is used to perform the reflection about the state, is essential to quantify the error in the algorithm. The following result describes the eigenphases of \mathcal{U} .

Lemma 3. (Eigenspectra of walk operator) *Let \hat{F} be an observable ($\|\hat{F}\|_{\text{op}} \leq 1$) and H be a Hamiltonian ($\|H\|_{\text{op}} \leq 1$). Consider the unitary $\mathcal{U} := (\text{c-}\mathcal{B}[\hat{F}]) \cdot (\text{c-}R_{\tilde{\psi}_{0,+}})$, a rotation constructed from two controlled reflections.*

Then \mathcal{U} has eigenphases $\theta_{0,\pm} = \pm \frac{1}{2\pi} \cos^{-1}(2|\omega|^2 - 1)$ where

$$\frac{1}{4} \langle\sigma_0|\mathbb{1} - \hat{F}|\sigma_0\rangle_{\text{sys}} |\langle\rho_0^+|0\rangle_{\text{iph}}|^2 - \nu \leq |\omega|^2 \leq \frac{1}{4} \langle\sigma_0|\mathbb{1} - \hat{F}|\sigma_0\rangle_{\text{sys}} |\langle\rho_0^+|0\rangle_{\text{iph}}|^2 + \nu;$$

$$\nu := 2|\langle\rho_0^+|0\rangle| \max_{j>0,\pm} \left\{ \left| \langle 0|\rho_j^\pm \rangle_{\text{iph}} \right|, \left| \langle 0|\rho_0^- \rangle_{\text{iph}} \right| \right\},$$

with $|\rho_j^\pm\rangle_{\text{iph}} = \frac{1}{\sqrt{2^n}} \sum_{a,x=0}^{2^n-1} W_a^*(x) e^{-2\pi i(\phi_{j,\pm} - \tilde{\phi}_{0,+})x} |a\rangle_{\text{iph}}$. $\text{c-}\mathcal{B}[\hat{F}]$ denotes the block encoding $\mathcal{B}[\hat{F}]$ controlled on the $|00\rangle_{\text{iph},\mathcal{B}_H}$ subspace. $|\sigma_0\rangle_{\text{sys}}$ is the groundstate of H with the eigenphase $\phi_{0,+}$ corresponding to the positive branch of the qubitised encoding of the Hamiltonian $\mathcal{Q}[H]$. The reflection $R_{\tilde{\psi}_{0,+}}$ (Eq. (8)) is controlled on the $|0\rangle_{\mathcal{B}_F}$ subspace and implemented using a coherent QPE with n phase qubits prepared by \hat{W} .

The proof of Lemma 3 is given in Appendix A. With an exact reflection the above resembles Theorem 2, $|\omega|^2 = \frac{|\langle \rho_0^+ | 0 \rangle_{\text{iph}}|^2}{4} \langle \sigma_0 | \mathbb{1} - \hat{F} | \sigma_0 \rangle$ ⁴. Without making any assumptions about the distribution of the Hamiltonian spectra, Lemma 3 describes the propagated effect of the imperfect iQPE on the iterate. The error depends on the overlap $|\langle 0 | \rho_j^\pm \rangle|$ which is affected by: the number of qubits n in the QPE, the state preparation \hat{W} and the phase difference $(\phi_{j,\pm} - \tilde{\phi}_{0,+})$.

For a useful algorithm, the Hamiltonian is assumed to have a known lower bound on the spectra gap δ so that the ground state can be distinguished. The Hamiltonian is then sub-normalised during the block encoding so that the maximum eigenvalue of the block encoded operator is $(1 - \delta_r)$ where $\delta_r = \delta / \|H\|_{\text{op}}$ is the relative spectral gap. The assumption also implies a known lower bound on the phase gap $\delta_\phi = |\phi_{1,+} - \phi_{0,+}|$ for the qubitised Hamiltonian.

The size of the inner phase register is determined by the phase gap. Let l be the minimum number of qubits required to resolve the phase gap, and add m extra qubits to the inner phase register to improve the performance so that the total is $n = l + m$. To successfully target the reflection, the reflected phase must be the closest finite bit representation of the true eigenphase of $|\psi_{0,+}\rangle$ i.e. $|\phi_{0,+} - \tilde{\phi}_{0,+}| < \frac{1}{2^{l+m}}$ and all other eigenphases are well separated from the reflected phase $|\phi_{1,+} - \tilde{\phi}_{0,+}| > \frac{1}{2^{l+m}}$ for all m . These two conditions give us the following relationship between the spectral gap promise and the number of qubits $\delta_\phi > \frac{1+2^m}{2^{l+m}}$. This ensures that $|\langle 0 | \rho_j^\sigma \rangle|$ is close to 1 only when $j = 0$ and $\sigma = +$ and close to zero for *all excited states*. The overlap can be suppressed for states well separated from $\tilde{\phi}_{0,+}$ by increasing m , illustrated by Fig. 3 for the rectangular window. This figure also illustrates that the value of the overlap for contaminating states depends less on the absolute difference in phase $|\phi - \tilde{\phi}_{0,+}|$ more on whether the difference is close to a $(l + m)$ -bit representation. Therefore, only considering the low energy excited states does not give an accurate estimate of the error and we analyse the full Hamiltonian spectrum to accurately describe the error.

The overlap value also depends on the choice of phase preparation unitary \hat{W} . Since aside from the spectral gap we assume no knowledge of the Hamiltonian spectrum by choosing a tapered function – such as the Kaiser window (Eq. (4)) – this overlap can be suppressed for all excited states. This is done by increasing the tunable bandwidth parameter β to suppress the DFT side-band amplitude at the expense of widening the central lobe – refer back to Fig. 1. Complexity analysis [4] shows that in the asymptotic limit increasing β exponentially suppresses the QPE failure probability.⁵ In practice, when there is a finite phase register there is a trade-off to be found when choosing β : increasing β suppresses the side bands so initially decreases the value of the overlap, however if β is increased further the central lobe widens enough to extend past the spectral gap region and increase the value of the overlap. One method for choosing β for a given l and m is by matching the width of the central lobe to the spectral gap region. The width of the central lobe is given by the first minima of the DFT:

Claim 4. *Consider that a window-enhanced QPE is used to reflect about the ground state of a qubitised Hamiltonian with spectral phase gap lower bounded by 2^{-l} . The $(l + m)$ -qubit phase register of a QPE is prepared in the superposition $\sum_{x=-(N-1)/2}^{(N-1)/2} K(x, \beta) |x\rangle$ where $K(x, \beta) \propto I_0(\beta \sqrt{1 - (x/2N)^2})$ is the Kaiser function with bandwidth β and $N = 2^{l+m}$. The value of β that minimises the contamination error from excited states is*

$$\beta_{\text{opt}} = \pi \sqrt{2^{2m} - 1}. \quad (12)$$

Proof. The Fourier transform of the Kaiser function is proportional to $\text{sinc}[\sqrt{(N\omega/2)^2 - \beta^2}]$. Therefore, the first minima of the Fourier transform occurs at $\sqrt{(N\omega_{\text{min}}/2)^2 - \beta^2} = \pi$. Solving for ω_{min} ,

⁴The additional factor of $|\langle \rho_0^+ | 0 \rangle_{\text{iph}}|^2$ is a result of the extra control added to the observable block encoding. In the case of an infinite QPE phase register $|\langle \rho_0^+ | 0 \rangle_{\text{iph}}|^2 \rightarrow 1$.

⁵The error in Lemma 3 is connected to the maximum value of the overlap outside of the spectral gap region. The plot of the overlap squared corresponds to the success probability in simple QPE, therefore the failure probability that is exponentially suppressed here corresponds to the areas under the curve outside of the spectral gap region – a related but different quantity to that which is studied here.

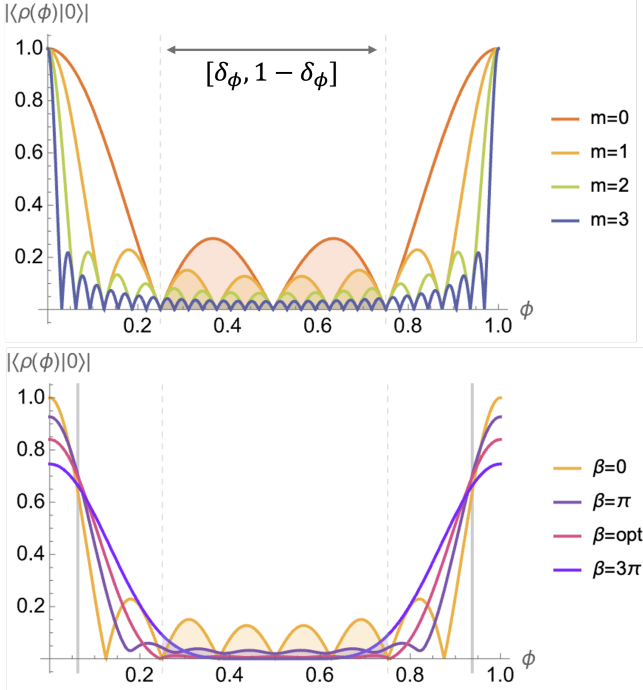


Figure 3: Plot of the behaviour of the overlap, $|\langle \rho(\phi) | 0 \rangle|$, for different phase register size and preparation. Recall that $|\rho(\phi)\rangle$ is defined in Eq. (10) and corresponds to the state of the phase register after performing a QPE and a reflection on the phase register. The maximum absolute value of the overlap appears in the error bound in Lemma 3. The spectral gap of the Hamiltonian ensures that for the error bound only the overlap in the range $[\delta_\phi, 1 - \delta_\phi]$ needs to be considered. The dashed grey lines demarcate this cut off where $\delta_\phi = 1/2^l$ where l is the minimum number of phase qubits, and the region contributing to the error is shaded under the curve. The smaller the maximum value of the overlap in the shaded region the more accurate the QPE implementation of the reflection. **Top:** Adding additional phase register qubits reduces the overlap given a rectangular window. The total number of phase qubits is $n = l + m$, and the phase register is prepared in uniform superposition. **Bottom:** Preparing the phase register of the QPE in a Kaiser window reduces the overlap. The number of phase qubits is fixed with $m = 1$. Increasing β widens the central lobe and suppresses the side-bands of the overlap function. There is a close to optimal β taken from Claim 4 that reduces the overlap maximum above the dashed line. The thick grey line demarcates the maximum value of $|\phi_0^+ - \tilde{\phi}_0^+|$.

the phase of the first minima in the DFT ϕ_k is given by

$$2\pi\phi_K = \sqrt{4(\pi^2 + \beta^2)}/N.$$

Matching $\phi_K = \frac{1}{2^l}$ gives an analytic expression for the ‘optimal’ β . \square

For $m > 0$ a non-zero value for β outperforms the rectangular function⁶ as seen in Fig. 3. This optimal bandwidth scales as $\beta \in O(2^m)$ as expected from the complexity analysis in [4]. Optimality is quoted since in practice the best β to minimise the resource count will depend on several factors not only minimising overlap, for example increasing β also has the effect of reducing the peak amplitude at null phase difference and may be harder to calculate and prepare the state. To optimise resource counts for real applications it could be beneficial to set a maximum value of β and follow Claim 4

⁶Generally at least one extra qubit is required to determine the phase [32].

only up to this threshold due to the expense of preparing a high β window function on many qubits, this is done to obtain the resource estimates in later sections.

2.2 Error and success probability

This section analyses the error and success probability of Algorithm 1, starting with the error analysis. There are several sources of error inherent to the algorithm arising from finite register size, even assuming perfect gate implementations and exact state preparation routines. With these assumptions, algorithmically the error in the final expectation value estimate is a combination of contributions: *reflection error*, from the imperfect implementation of the state reflection due to the finite iQPE phase register; *oQPE error*, from the imprecision in the output due to the oQPE and *pre-learning error* from learning the value of $|\langle \rho_0^+ | 0 \rangle|^2$. These error contributions amalgamate in the following algorithmic error bound.

Proposition 5. (Expectation value algorithm error analysis) *A successful instance of Algorithm 1 outputs an ϵ -approximation of $\langle \sigma_0 | \hat{F} | \sigma_0 \rangle$ where*

$$\epsilon \leq \frac{3\pi 2^{-n_o} + 8|\langle \rho_0^+ | 0 \rangle| \max_{j>0,\pm} \{|\langle 0 | \rho_j^\pm \rangle|, |\langle 0 | \rho_0^- \rangle|\} + c}{|\langle \rho_0^+ | 0 \rangle|^2},$$

given $|\rho_j^\pm\rangle_{\text{iph}} := \frac{1}{\sqrt{2^n}} \sum_{a,x=0}^{2^n-1} W_a^*(x) e^{-2\pi i(\phi_{j,\pm} - \tilde{\phi}_{0,+})x} |a\rangle_{\text{iph}}$, the number of qubits in the phase register of the oQPE is n_o and c is a free non-negative constant.

Proof of Proposition 5 deferred to Appendix A

The free constant c appears in the bounds for both the error and the success probability – hence there is a tradeoff to be considered when setting its value. This error bound is needed to estimate the computational resources of the algorithm in Section 3. The success probability of the algorithm can also be bounded:

Proposition 6. (Expectation value algorithm success probability) *Algorithm 1 succeeds with probability,*

$$p_{\text{success}} \geq |\langle 0 | \rho_0^+ \rangle|^2 \left(1 - \frac{32 \max_{j>0,\pm} \{|\langle 0 | \rho_j^\pm \rangle|, |\langle 0 | \rho_0^- \rangle|\}^2}{c} \right),$$

where $|\rho_j^\pm\rangle_{\text{iph}} := \frac{1}{\sqrt{2^n}} \sum_{a,x=0}^{2^n-1} W_a^*(x) e^{-2\pi i(\phi_{j,\pm} - \tilde{\phi}_{0,+})x} |a\rangle_{\text{iph}}$ and c is the free non-negative constant from the error tolerance.

Referring to Fig. 3 if the system is gapped and an appropriate number of QPE qubits are used this ensures $\max_{(j,\sigma)\neq(0,+)} \{|\langle 0 | \rho_j^\pm \rangle|, |\langle 0 | \rho_0^- \rangle|\}$ is small and the success probability is close to 1. See Appendix A for the full proof of Proposition 6. The free constant c in the error and success probability can be freely tuned, but for example if $c = |\langle \rho_0^+ | 0 \rangle| \max_{j>0,\pm} \{|\langle 0 | \rho_j^\pm \rangle|, |\langle 0 | \rho_0^- \rangle|\}$ then

$$\epsilon \leq \frac{3\pi 2^{-n_o} + 9|\langle \rho_0^+ | 0 \rangle| \max_{j>0,\pm} \{|\langle 0 | \rho_j^\pm \rangle|, |\langle 0 | \rho_0^- \rangle|\}}{|\langle \rho_0^+ | 0 \rangle|^2} \quad (13)$$

$$p_{\text{success}} \geq |\langle 0 | \rho_0^+ \rangle|^2 \left(1 - \frac{32 \max_{j>0,\pm} \{|\langle 0 | \rho_j^\pm \rangle|, |\langle 0 | \rho_0^- \rangle|\}}{|\langle 0 | \rho_0^+ \rangle|} \right). \quad (14)$$

3 Algorithm resource estimates

Proposition 5 shows that the final error in the expectation value is comprised of an error due to the oQPE (that is reduced by increasing the number of oQPE phase qubits) and an error due to the reflection about the eigenstate (that is reduced by either increasing the number of iQPE phase qubits or using QSP). When using the Kaiser window there is a reduction in gate count that originates from reducing this reflection error. Fig. 4 illustrates that for the same number of quantum resources, a Kaiser window function with optimal bandwidth achieves a lower error in the reflection implementation than a rectangular window and QSP-rounded QPE for a large range of relative errors. While the scaling of the QPE with window functions is still linear (whereas with QSP the error decreases exponentially with the increased resources) the constants involved lead to window functions outperforming QSP for most practical cases.

As a case study for the use of window functions in coherent QPE, we demonstrate that constant factor resource estimates for the expectation value estimation algorithm can be significantly reduced by using the Kaiser window function. The expectation value of both one and two body observables are considered with respect to the ground state of different molecular systems. For the benchmark dataset we selected three closed-shell molecules — water, ammonia, and p-benzene — treating each in the all-electron picture with a cc-pVDZ basis set. Additionally, we consider a cytochrome P450 heme model in an open-shell configuration, using a (42e, 43o) active space in the cc-pVDZ basis targeting the $S = 1$ spin state. In previous work, this active space model was chosen to elucidate the mechanism by which artemisinin binds to heme [11, 34].

To produce a resource estimate of the expectation value algorithm, the Hamiltonian of the given molecular system must be block-encoded. In previous work, double factorisation was used to block-encode both the electronic structure Hamiltonian and relevant observables [40], however, further cost reductions may be achieved with symmetry-shifting or block-invariant symmetry-shifting (BLISS) techniques [37, 26, 12]. This work advocates for the use of tensor hypercontraction (THC) which has been shown to provide improved resource reduction in the estimation of molecular energies [25, 8], and finds that BLISS-THC provides a significant improvement in the block-encoding cost for observable estimation compared to previous approaches. The tensor factorization procedure was adapted to the expectation value algorithm by concurrently optimizing the rank of the Hamiltonian and observable with respect to a precision budget which estimates the error of the expectation value obtained by the truncated Hamiltonian and truncated observable against that of their respective untruncated versions using coupled cluster calculations with singles and doubles (CCSD) [41]. Details of the procedure may be found in Appendix B.2. This strategy leads to a further reduction in the overall costs in comparison to previous numeric end-to-end resource estimates for this routine [40], evidenced by the rectangular window and QSP-rounded traces.

The complete quantum resource estimation for this algorithm in terms of Toffoli gate counts is plotted in Fig. 5 for various molecules and observables including the kinetic energy, electric dipole moment, and electron repulsion interaction operators. The target error tolerances used are $\epsilon_{\text{kin.}} = 1.6 \text{ mHa}$, $\epsilon_{\text{dip.}} = 10 \text{ mDebye}$ and $\epsilon_{\text{eri}} = 1.6 \text{ mHa}$ consistent with common literature values. Appendix B gives more details into how these resource estimates are calculated. For all algorithm variants the gate count increases with the complexity of the molecule as expected, but a significant reduction is seen using window-assisted iQPE compared to QSP rounding — in the largest system an almost 2-orders-of-magnitude reduction in the Toffoli count is observed. Compared to the naive implementation of QPE, the proposed routine represents a reduction in the Toffoli gate count by more than five orders of magnitude.

The logical qubit cost of the algorithm scales linearly with the Hamiltonian size — estimates given in Table 1. The qubit count is largely comparable across the different variations since the qubit cost is dominated by the block encoding ancilla requirements. The rectangular window case requires systematically slightly more qubits than the other variants, and the QSP estimate is slightly marginally lower (5 less) than the window case. Future work will examine how data batching and additional space-time trade-offs in the block-encoding of the Hamiltonian and observables can further reduce

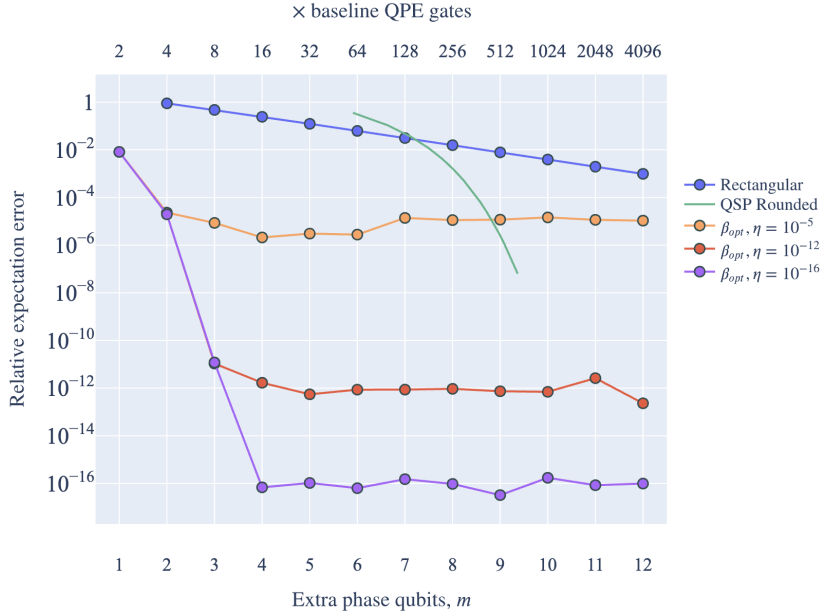


Figure 4: Plot of the relative expectation error arising from the reflection implementation. Standard QPE (‘Rectangular’) and using QSP to round the QPE (‘QSP rounded’) is compared to Kaiser window-enhanced QPE proposed in this work with optimal bandwidth. Three Kaiser window cases are plotted with varying error in the state preparation, η . In the standard and Kaiser window-enhanced versions, the error is reduced by adding qubits to the phase register. The size of the phase register determines the number of calls to the controlled unitary (in this case the block encoded Hamiltonian), hence this reduction in error leads to increased gate count reflected by the top x axis. In the QSP case the error is reduced by performing a higher degree polynomial, this also corresponds to increasing the quantum resources but does not effect the size of the phase register, hence only the top x axis corresponds to the QSP curve (opposed to the other traces where both x -axis apply). The QSP curve represents the minimum error achievable, but in practice finding the phase angles to the required accuracy may be challenging. One baseline QPE query corresponds to the number of quantum gates required to perform QPE on the system with the minimum number phase qubits sufficient to discern the ground state. Increasing the number of phase qubits linearly decreases the relative expectation error on the log plot, in the Kaiser case the linear trend is disrupted when the relative error is comparable with the state preparation error. While the QSP rounded version decreases exponentially according to the emulation, in practice requires heavy classical pre-processing to calculate phase angles. Nevertheless due to much steeper gradient of the linear Kaiser window curve, the window-enhanced version also outperforms QSP for most practical cases.

the logical-qubit count.

4 Conclusions

This work builds on [24, 33, 40] to present an adapted expectation value estimation algorithm that employs window-assisted coherent QPE. This modification results in improved algorithmic-error-to-quantum-resources ratio that can be seen in Fig. 3. Since QPE is one of the small handful of elemental quantum routines, we hope this analysis will act as a model for how window-assisted coherent QPE can be used as a subroutine and lead to reduced overall errors, for instances in other cases where reflection about an eigenstate is used. Additionally the classical preprocessing of the block encodings

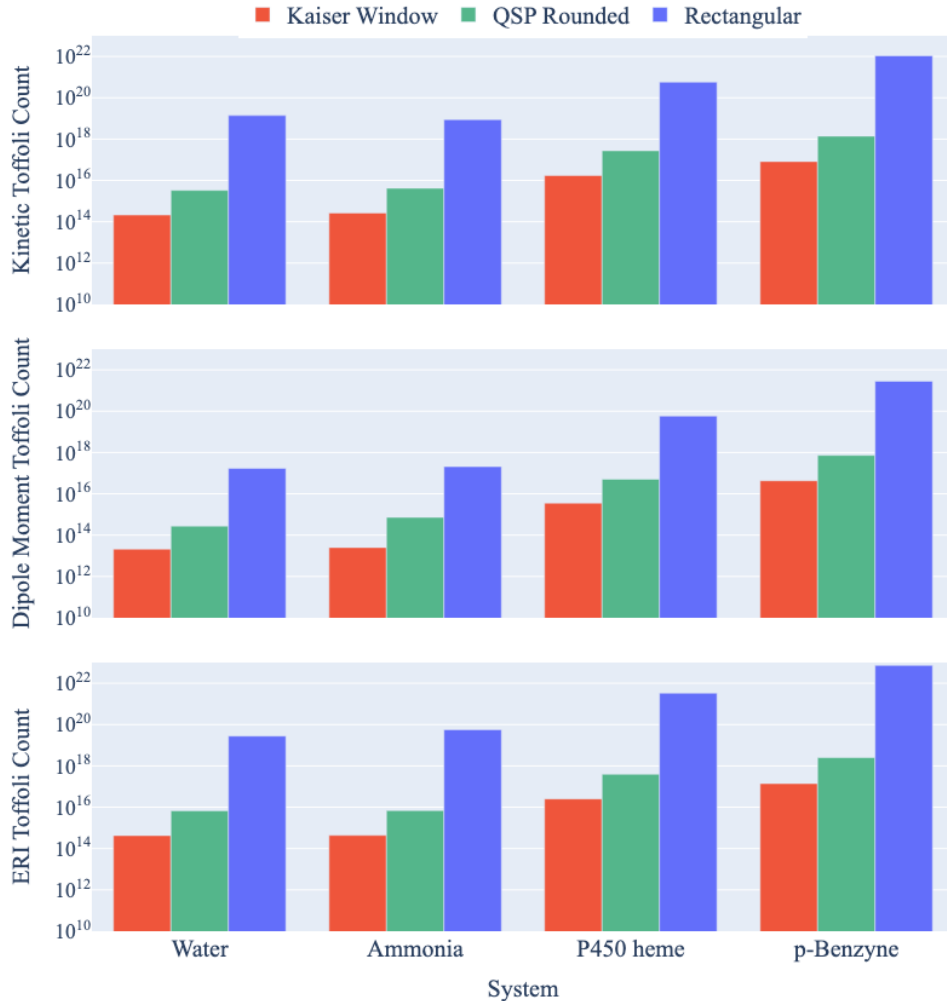


Figure 5: Resource estimates for the expectation value algorithm for a variety of systems: water, ammonia, p-Benzene, P450 heme; and a variety of observables: kinetic energy, dipole moment and electron repulsion integral (ERI). The left axis denotes the estimated number of Toffolis gates required for the expectation value algorithm. Three methods for implementing the inner QPE also depicted in Fig. 4 are given to demonstrate the impact on the overall algorithm of having a higher success amplitude in the coherent QPE. For all Hamiltonian block-encodings BLISS-THC is used, as well as for ERI the two-body observable.

of the Hamiltonian and observable together for expectation value estimation is novel to this work and highlights the potential for further optimisation of error budgeting. While estimating molecular observables is still an expensive algorithm, the ability to produce end-to-end resource estimates and see these estimates reduced is very encouraging and a further step on the path towards closing the gap between commercially interesting applications and hardware capabilities.

System	Observable	Logical qubits		
		Rectangular	QSP rounded	Kaiser window
Water	KE	520	499	504
	x -dipole	429	411	416
	ERI	518	497	502
Ammonia	KE	628	608	613
	x -dipole	494	477	481
	ERI	586	564	569
P450 heme	KE	1096	1076	1081
	x -dipole	910	891	896
	ERI	819	797	802
p-Benzyne	KE	2646	2624	2629
	x -dipole	2708	2687	2692
	ERI	2582	2558	2563

Table 1: Table of logical qubit highwater for the algorithm. Various subroutines require local ancilla that are uncomputed at the end of the subroutine so can be reused for later routines, the logical qubit highwater corresponds to the maximum number of logical qubits required in parallel at any point in the algorithm. Details of this estimation are given in Appendix B.

Acknowledgments

The authors would like to thank the team at PsiQuantum for various discussions and support. The work was facilitated by access to PsiQuantum software suit including the visualisation tools which produced Fig. 2a.

References

- [1] Scott Aaronson. Shadow tomography of quantum states. *SIAM Journal on Computing*, 49(5):STOC18–368–STOC18–394, 2020.
- [2] Ryan Babbush, Dominic W. Berry, Robin Kothari, Rolando D. Somma, and Nathan Wiebe. Exponential quantum speedup in simulating coupled classical oscillators. *Phys. Rev. X*, 13:041041, Dec 2023.
- [3] Ryan Babbush, Craig Gidney, Dominic W. Berry, Nathan Wiebe, Jarrod McClean, Alexandru Paler, Austin Fowler, and Hartmut Neven. Encoding electronic spectra in quantum circuits with linear t complexity. *Phys. Rev. X*, 8:041015, Oct 2018.
- [4] Dominic W. Berry, Yuan Su, Casper Gyurik, Robbie King, Joao Basso, Alexander Del Toro Barba, Abhishek Rajput, Nathan Wiebe, Vedran Dunjko, and Ryan Babbush. Analyzing prospects for quantum advantage in topological data analysis. *PRX Quantum*, 5:010319, Feb 2024.
- [5] Dominic W. Berry, Yu Tong, Tanuj Khattar, Alec White, Tae In Kim, Sergio Boixo, Lin Lin, Seunghoon Lee, Garnet Kin-Lic Chan, Ryan Babbush, and Nicholas C. Rubin. Rapid initial state preparation for the quantum simulation of strongly correlated molecules, 2024.
- [6] R. Bhatia. *Matrix Analysis*. Graduate Texts in Mathematics. Springer New York, 1996.
- [7] Gilles Brassard, Peter Høyer, Michele Mosca, and Alain Tapp. Quantum amplitude amplification and estimation, 2002.

- [8] Athena Caesura, Cristian L. Cortes, William Pol, Sukin Sim, Mark Steudtner, Gian-Luca R. Anselmetti, Matthias Degroote, Nikolaj Moll, Raffaele Santagati, Michael Streif, and Christofer S. Tautermann. Faster quantum chemistry simulations on a quantum computer with improved tensor factorization and active volume compilation, 2025.
- [9] A.B. Carlson and P.B. Crilly. *Communication Systems: An Introduction to Signals and Noise in Electrical Communication*. Higher education/ [Mcgraw-Hill]. McGraw-Hill, 2010.
- [10] Clusius. Einführung in die quantenchemie. von h. hellmann. 350 s.,43 abb., 35 tab. franz deuticke, leipzig u. wien 1937. pr. geh. rm. 20,-. geb. rm. 22,-. *Angewandte Chemie*, 54:156–156, 1941.
- [11] Cristian L Cortes, Matthias Loipersberger, Robert M Parrish, Sam Morley-Short, William Pol, Sukin Sim, Mark Steudtner, Christofer S Tautermann, Matthias Degroote, Nikolaj Moll, et al. Fault-tolerant quantum algorithm for symmetry-adapted perturbation theory. *PRX Quantum*, 5(1):010336, 2024.
- [12] Konrad Deka and Emil Zak. Simultaneously optimizing symmetry shifts and tensor factorizations for cost-efficient fault-tolerant quantum simulations of electronic hamiltonians. *Journal of Chemical Theory and Computation*, 21(9):4458–4465, 05 2025.
- [13] Yulong Dong, Xiang Meng, K. Birgitta Whaley, and Lin Lin. Efficient phase-factor evaluation in quantum signal processing. *Phys. Rev. A*, 103:042419, Apr 2021.
- [14] I.A.I. Frenkel. *Wave Mechanics: Advanced General Theory*. Number v. 2 in International series of monographs on physics. Clarendon Press, 1934.
- [15] András Gilyén, Yuan Su, Guang Hao Low, and Nathan Wiebe. Quantum singular value transformation and beyond: exponential improvements for quantum matrix arithmetics. In *Proceedings of the 51st Annual ACM SIGACT Symposium on Theory of Computing*, STOC 2019, page 193–204, New York, NY, USA, 2019. Association for Computing Machinery.
- [16] Sean Greenaway, William Pol, and Sukin Sim. A case study against qsvt: assessment of quantum phase estimation improved by signal processing techniques, 2024.
- [17] Lov Grover and Terry Rudolph. Creating superpositions that correspond to efficiently integrable probability distributions, 2002.
- [18] Jeongwan Haah. Product Decomposition of Periodic Functions in Quantum Signal Processing. *Quantum*, 3:190, October 2019.
- [19] F.J. Harris. On the use of windows for harmonic analysis with the discrete fourier transform. *Proceedings of the IEEE*, 66(1):51–83, 1978.
- [20] Trygve Helgaker, Sonia Coriani, Poul Jørgensen, Kasper Kristensen, Jeppe Olsen, and Kenneth Ruud. Recent advances in wave function-based methods of molecular-property calculations. *Chemical Reviews*, 112(1):543–631, 2012. PMID: 22236047.
- [21] Hsin-Yuan Huang, Richard Kueng, and John Preskill. Predicting many properties of a quantum system from very few measurements. *Nature Physics*, 16(10):1050–1057, 2020.
- [22] William J Huggins, Kianna Wan, Jarrod McClean, Thomas E O'brien, Nathan Wiebe, and Ryan Babbush. Nearly optimal quantum algorithm for estimating multiple expectation values. *Physical Review Letters*, 129, 2022.
- [23] J. Kaiser and R. Schafer. On the use of the i0-sinh window for spectrum analysis. *IEEE Transactions on Acoustics, Speech, and Signal Processing*, 28(1):105–107, 1980.

- [24] Emanuel Knill, Gerardo Ortiz, and Rolando D. Somma. Optimal quantum measurements of expectation values of observables. *Phys. Rev. A*, 75:012328, Jan 2007.
- [25] Joonho Lee, Dominic W. Berry, Craig Gidney, William J. Huggins, Jarrod R. McClean, Nathan Wiebe, and Ryan Babbush. Even more efficient quantum computations of chemistry through tensor hypercontraction. *PRX Quantum*, 2:030305, Jul 2021.
- [26] Ignacio Loaiza and Artur F Izmaylov. Block-invariant symmetry shift: Preprocessing technique for second-quantized hamiltonians to improve their decompositions to linear combination of unitaries. *Journal of Chemical Theory and Computation*, 19(22):8201–8209, 2023.
- [27] Guang Hao Low and Isaac L. Chuang. Hamiltonian Simulation by Qubitization. *Quantum*, 3:163, July 2019.
- [28] Guang Hao Low, Vadym Kliuchnikov, and Luke Schaeffer. Trading T gates for dirty qubits in state preparation and unitary synthesis. *Quantum*, 8:1375, June 2024.
- [29] Nikhil S. Mande and Ronald de Wolf. Tight bounds for quantum phase estimation and related problems. *Leibniz International Proceedings in Informatics, LIPIcs*, 274, 5 2023.
- [30] Sam McArdle, András Gilyén, and Mario Berta. Quantum state preparation without coherent arithmetic, 2025.
- [31] Daniel Nagaj, Paweł Wocjan, and Yong Zhang. Fast amplification of QMA, 2009.
- [32] M.A. Nielsen and I.L. Chuang. *Quantum Computation and Quantum Information: 10th Anniversary Edition*. Cambridge University Press, 2010.
- [33] Thomas E O'brien, Michael Streif, Nicholas C Rubin, Raffaele Santagati, Yuan Su, William J Huggins, Joshua J Goings, Nikolaj Moll, Elica Kyoseva, Matthias Degroote, Christofer S Tautermann, Joonho Lee, Dominic W Berry, Nathan Wiebe, and Ryan Babbush. Efficient quantum computation of molecular forces and other energy gradients. *Physical Review Research*, 4, 2022.
- [34] Gary H Posner and Paul M O'Neill. Knowledge of the proposed chemical mechanism of action and cytochrome p450 metabolism of antimalarial trioxanes like artemisinin allows rational design of new antimalarial peroxides. *Accounts of chemical research*, 37(6):397–404, 2004.
- [35] Patrick Rall. Quantum algorithms for estimating physical quantities using block encodings. *Phys. Rev. A*, 102:022408, Aug 2020.
- [36] Patrick Rall. Faster Coherent Quantum Algorithms for Phase, Energy, and Amplitude Estimation. *Quantum*, 5:566, October 2021.
- [37] Dario Rocca, Cristian L. Cortes, Jérôme F. Gonthier, Pauline J. Ollitrault, Robert M. Parrish, Gian-Luca Anselmetti, Matthias Degroote, Nikolaj Moll, Raffaele Santagati, and Michael Streif. Reducing the runtime of fault-tolerant quantum simulations in chemistry through symmetry-compressed double factorization. *Journal of Chemical Theory and Computation*, 20(11):4639–4653, 2024. PMID: 38788209.
- [38] Sébastien Roch. Matrix perturbation theory: Math 833 modern discrete probability, 2020.
- [39] Yuval R. Sanders, Dominic W. Berry, Pedro C.S. Costa, Louis W. Tessler, Nathan Wiebe, Craig Gidney, Hartmut Neven, and Ryan Babbush. Compilation of fault-tolerant quantum heuristics for combinatorial optimization. *PRX Quantum*, 1:020312, Nov 2020.

- [40] Mark Steudtner, Sam Morley-Short, William Pol, Sukin Sim, Cristian L. Cortes, Matthias Loipersberger, Robert M. Parrish, Matthias Degroote, Nikolaj Moll, Raffaele Santagati, and Michael Streif. Fault-tolerant quantum computation of molecular observables. *Quantum*, 7:1164, November 2023. Published 2023-11-06.
- [41] Qiming Sun, Xing Zhang, Samragni Banerjee, Peng Bao, Marc Barbry, Nick S Blunt, Nikolay A Bogdanov, George H Booth, Jia Chen, Zhi-Hao Cui, et al. Recent developments in the pyscf program package. *The Journal of chemical physics*, 153(2), 2020.
- [42] M. Szegedy. Quantum speed-up of markov chain based algorithms. In *45th Annual IEEE Symposium on Foundations of Computer Science*, pages 32–41, 2004.
- [43] Terrance Tao. <https://terrytao.wordpress.com/2010/01/12/254a-notes-3a-eigenvalues-and-sums-of-hermitian-matrices/>, 2024.

Appendices

A Deferred proofs

To aid the readability of the main text, the proofs of the claims are collated here, including some intermediate technical results that are used in the proofs.

A.1 Proof of Lemma 1

The rest of the proofs make good use of the following general result about the product of two reflections:

Lemma 1. *[[42] or [31, Appendix A]] Consider two reflections:*

$$R_A = \mathbb{1} - 2\Pi_A \quad \text{and} \quad R_B = \mathbb{1} - 2\Pi_B,$$

where ω_k are the singular values of the projector product $\Pi_A \cdot \Pi_B$. The product of these reflections $\mathcal{U} := R_B R_A$ is a unitary with eigenphases:

$$\theta_{k,\pm} = \mp \frac{1}{2\pi} \cos^{-1} \left(2|\omega_k|^2 - 1 \right).$$

Proof. Jordan's lemma [6, Chapter VII] tells us that given any two projectors Π_A and Π_B the Hilbert space can be block diagonalised into two-dimensional subspaces S_k invariant under the action of both projectors and one-dimensional subspaces T_j on which $\Pi_A \Pi_B$ acts as either the identity of the null projector. The projectors can then be expressed in the basis that respects this block diagonal structure:

$$\Pi_A = \sum_k |a_k\rangle\langle a_k| \otimes |k\rangle\langle k| + \pi_B^\perp \quad \text{and} \quad \Pi_B = \sum_k |b_k\rangle\langle b_k| \otimes |k\rangle\langle k| + \pi_A^\perp,$$

where $\langle b_k|a_k\rangle = \omega_k \in \mathbb{R}$ and $\langle k|j\rangle = \delta_{j,k}$. Additionally π_A^\perp (π_B^\perp) is orthogonal to $\sum_k |k\rangle\langle k|$ and Π_A (Π_B). Each subspace S_k is spanned both by $\{|a_k\rangle, |a_k^\perp\rangle\}$ and $\{|b_k\rangle, |b_k^\perp\rangle\}$ where $|a_k^\perp\rangle = \frac{1}{\sqrt{1-\omega_k^2}} (\mathbb{1} - |a_k\rangle\langle a_k|) |b_k\rangle$ and vice versa. So we have the relation $|b_k\rangle = \omega_k |a_k\rangle + \bar{\omega}_k |a_k^\perp\rangle$ where $\bar{\omega}_k = \sqrt{1-|\omega_k|^2}$. With this structure in place we can analyse the action of $\mathcal{U} = R_B R_A$:

$$\mathcal{U} = \left(\mathbb{1} - 2 \left(\sum_k |b_k\rangle\langle b_k| \otimes |k\rangle\langle k| \right) + \pi_A^\perp \right) \cdot \left(\mathbb{1} - 2 \left(\sum_k |a_k\rangle\langle a_k| \otimes |k\rangle\langle k| \right) + \pi_B^\perp \right) \quad (15a)$$

$$= \mathbb{1} + \sum_k (4\omega_k |b_k\rangle\langle a_k| - 2|b_k\rangle\langle b_k| - 2|a_k\rangle\langle a_k|) \otimes |k\rangle\langle k| - 2\pi_A^\perp - 2\pi_B^\perp \quad (15b)$$

$$= \mathbb{1} + \sum_k \left(4\omega_k (\omega_k |a_k\rangle + \bar{\omega}_k |a_k^\perp\rangle) \langle a_k| - 2(\omega_k |a_k\rangle + \bar{\omega}_k |a_k^\perp\rangle) (\omega_k \langle a_k| + \bar{\omega}_k \langle a_k^\perp|) - 2|a_k\rangle\langle a_k| \right) \otimes |k\rangle\langle k| - 2\pi_A^\perp - 2\pi_B^\perp \quad (15c)$$

Then we show that the following states are eigenstates of \mathcal{U} :

$$|v_{k,\pm}\rangle = \frac{1}{\sqrt{2}} \left(|a_k\rangle \pm i|a_k^\perp\rangle \right) \otimes |k\rangle \quad (16)$$

with eigenphases given by the stated result.

$$\mathcal{U}|v_{k,\pm}\rangle = \mathcal{U}\frac{1}{\sqrt{2}}\left(|a_k\rangle \pm i|a_k^\perp\rangle\right) \otimes |k\rangle \quad (17a)$$

$$= \frac{1}{\sqrt{2}}\left(2|\omega_k|^2 - 1 \pm 2i\omega_k\bar{\omega}_k\right)|a_k\rangle \otimes |k\rangle \pm \frac{i}{\sqrt{2}}\left(2|\omega_k|_k - 1 \mp 2i\omega_k\bar{\omega}_k\right)|a_k^\perp\rangle \otimes |k\rangle \quad (17b)$$

$$= \left(2|\omega_k|^2 - 1 \mp 2i\omega_k\bar{\omega}_k\right)|v_{k,\pm}\rangle \quad (17c)$$

$$= (\cos(2\pi\theta_{k,\pm}) + i\sin(2\pi\theta_{k,\pm}))|v_{k,\pm}\rangle. \quad (17d)$$

Thus demonstrating that $|v_{k,\pm}\rangle$ is indeed an eigenvector of \mathcal{U} with eigenphase $\theta_{k,\pm}$. \square

A.2 Proof of Theorem 2

Theorem 2. Consider the walk operator $\mathcal{U} := (\mathcal{B}[\hat{F}]) \cdot (c\text{-}R_{\sigma_0})$ acting on $\mathcal{H}_{\text{sys}} \otimes \mathcal{H}_{\mathcal{B}_F}$ where $\mathcal{B}[\hat{F}]$ is a self-inverse block encoding of the renormalised observable \hat{F} ($\|\hat{F}\|_{\text{op}} \leq 1$) and $c\text{-}R_{\sigma_0}$ is the reflection about a groundstate, $|\sigma_0\rangle_{\text{sys}}$, controlled on the $|0\rangle_{\mathcal{B}_F}$ subspace. The state $|\sigma_0\rangle_{\text{sys}} \otimes |0\rangle_{\mathcal{B}_F}$ is an equal superposition of two eigenstates of \mathcal{U} with eigenphases,

$$\theta_{0,\pm} = \mp\frac{1}{2\pi}\cos^{-1}\left(\langle\sigma_0|\hat{F}|\sigma_0\rangle\right).$$

Proof. Let $c\text{-}R_{\sigma_0} = \mathbb{1} - 2|\sigma_0\rangle\langle\sigma_0|_{\text{sys}} \otimes |0\rangle\langle 0|_{\mathcal{B}_F}$ be the first reflection in Lemma 1 and $\mathcal{B}[\hat{F}] = \mathbb{1} - 2Q$ be the second. Hence we have the associated projectors $P := |a_0\rangle\langle a_0| = |\sigma_0\rangle\langle\sigma_0|_{\text{sys}} \otimes |0\rangle\langle 0|_{\mathcal{B}_F}$ and $Q := \frac{1}{2}(\mathbb{1} - \mathcal{B}[\hat{F}])$. The singular value decomposition of the product of projectors is

$$P \cdot Q = (|\sigma_0\rangle\langle\sigma_0|_{\text{sys}} \otimes |0\rangle\langle 0|_{\mathcal{B}_F}) \cdot \frac{1}{2}(\mathbb{1} - \mathcal{B}[\hat{F}]) = \sum_k \omega_k |a_k\rangle\langle b_k|. \quad (18)$$

The singular values can be found by considering the eigenvalues of the modulus square:

$$P \cdot Q \cdot Q^\dagger \cdot P^\dagger = P \cdot Q \cdot P \quad (19a)$$

$$= \langle\sigma_0|0|\frac{1}{2}(\mathbb{1} - \mathcal{B}[\hat{F}])|\sigma_0\rangle|0\rangle - |\sigma_0\rangle\langle\sigma_0|_{\text{sys}} \otimes |0\rangle\langle 0|_{\mathcal{B}_F} \quad (19b)$$

$$= \frac{1}{2}\left(1 - \langle\sigma_0|\hat{F}|\sigma_0\rangle\right) - |\sigma_0\rangle\langle\sigma_0|_{\text{sys}} \otimes |0\rangle\langle 0|_{\mathcal{B}_F} \quad (19c)$$

$$= |\omega_0|^2 |a_0\rangle\langle a_0|. \quad (19d)$$

This is a simple case since \hat{a} is a rank one projector with $|a_0\rangle = |\sigma_0\rangle_{\text{sys}}|0\rangle_{\mathcal{B}_F}$ and so there is only one non-trivial squared singular value $|\omega_0|^2 = \frac{1}{2}\left(1 - \langle\sigma_0|\hat{F}|\sigma_0\rangle\right)$. Along with Lemma 1 it follows that the only two eigenstates of \mathcal{U} with non-trivial eigenvalues are:

$$|v_\pm\rangle = \frac{1}{\sqrt{2}}\left(|\sigma_0\rangle_{\text{sys}}|0\rangle_{\mathcal{B}_F} \pm i|\perp\rangle\right) \quad (20)$$

with eigenphases $\theta_\pm = \mp\frac{i}{2\pi}\cos^{-1}\left(\langle\psi_0|\hat{F}|\psi_0\rangle\right)$. Then the statement is validated by noting the state's eigenvector decomposition $|\sigma_0\rangle_{\text{sys}}|0\rangle_{\mathcal{B}_F} = \frac{1}{\sqrt{2}}(|v_+\rangle + |v_-\rangle)$. \square

A.3 Proof of Lemma 3

Note that the unitary analysed below \mathcal{U} is depicted in the purple box of Fig. 2a.

Lemma 3. (Eigenspectra of walk operator) *Let \hat{F} be an observable ($\|\hat{F}\|_{\text{op}} \leq 1$) and H be a Hamiltonian ($\|H\|_{\text{op}} \leq 1$). Consider the unitary $\mathcal{U} := (\text{c-B}[\hat{F}]) \cdot (\text{c-}R_{\tilde{\psi}_0,+})$, a rotation constructed from two controlled reflections.*

Then \mathcal{U} has eigenphases $\theta_{0,\pm} = \pm \frac{1}{2\pi} \cos^{-1} (2|\omega|^2 - 1)$ where

$$\frac{1}{4} \langle \sigma_0 | \mathbb{1} - \hat{F} | \sigma_0 \rangle_{\text{sys}} |\langle \rho_0^+ | 0 \rangle_{\text{iph}}|^2 - \nu \leq |\omega|^2 \leq \frac{1}{4} \langle \sigma_0 | \mathbb{1} - \hat{F} | \sigma_0 \rangle_{\text{sys}} |\langle \rho_0^+ | 0 \rangle_{\text{iph}}|^2 + \nu;$$

$$\nu := 2|\langle \rho_0^+ | 0 \rangle| \max_{j>0,\pm} \left\{ \left| \langle 0 | \rho_j^\pm \rangle_{\text{iph}} \right|, \left| \langle 0 | \rho_0^- \rangle_{\text{iph}} \right| \right\},$$

with $|\rho_j^\pm\rangle_{\text{iph}} = \frac{1}{\sqrt{2^n}} \sum_{a,x=0}^{2^n-1} W_a^*(x) e^{-2\pi i(\phi_{j,\pm} - \tilde{\phi}_{0,+})x} |a\rangle_{\text{iph}}$. $\text{c-B}[\hat{F}]$ denotes the block encoding $\mathcal{B}[\hat{F}]$ controlled on the $|00\rangle_{\text{iph},\mathcal{B}_H}$ subspace. $|\sigma_0\rangle_{\text{sys}}$ is the groundstate of H with the eigenphase $\phi_{0,+}$ corresponding to the positive branch of the qubitised encoding of the Hamiltonian $\mathcal{Q}[H]$. The reflection $R_{\tilde{\psi}_0,+}$ (Eq. (8)) is controlled on the $|0\rangle_{\mathcal{B}_F}$ subspace and implemented using a coherent QPE with n phase qubits prepared by \hat{W} .

This proof of the above utilises the following intermediate results.

Claim 7. $\{|\psi_{i,\pm}\rangle | \rho(\phi_{i,\pm} - \frac{m}{2^n})\}_{i,\pm,m}$ is a complete orthogonal basis for $\mathcal{H}_{\text{sys}} \otimes \mathcal{H}_{\text{iph}} \otimes \mathcal{H}_{\mathcal{B}_H}$, where

$$\{|\psi_{i,\pm}\rangle := \frac{1}{\sqrt{2}} \left(\mathbb{1} \pm i \frac{\lambda_i \mathbb{1} - \mathcal{Q}[H]}{\sqrt{1 - \lambda_i}} \right) |\sigma_i\rangle_{\text{sys}} \otimes |0\rangle_{\mathcal{B}_H} \}$$

and

$$|\rho(y)\rangle_{\text{iph}} := \sum_{a=0}^{2^n-1} f(y, a) |a\rangle_{\text{iph}},$$

where $f(y, a) := \frac{1}{\sqrt{2^n}} \sum_{x=0}^{2^n-1} W_a^*(x) e^{-2\pi i y x}$ and $\{\sigma_i\}$ are the eigenvectors of an operator H acting in \mathcal{H}_{sys} with eigenvalues λ_i and $\mathcal{Q}[H]$ is a qubitised encoding of H .

Proof. $\langle \psi_{i,\pm} | \psi_{j,\pm'} \rangle = \delta_{i,j} \delta_{\pm,\pm'}$ by definition since $\{|\sigma\rangle_i\}$ is an orthonormal basis of \mathcal{H}_{sys} . All that is left to do is to demonstrate that for any given value of i and \pm , $\{|\rho(\phi_{i,\pm} - \frac{m}{2^n})\}_{m=0}^{2^n-1}$ forms an orthogonal basis for \mathcal{H}_{iph} . For $m, m' \in \mathbb{Z}^+ \in [0, 2^n-1]$ and all $\phi \in \mathbb{R}$ we have $\langle \rho(\phi - m/2^n) | \rho(\phi - m'/2^n) \rangle = \delta_{m,m'}$ since,

$$\langle \rho(\phi - m/2^n) | \rho(\phi - m'/2^n) \rangle = \sum_{a=0}^{2^n-1} f^*(\phi - \frac{m}{2^n}, a) f(\phi - \frac{m'}{2^n}, a) \quad (21a)$$

$$= \frac{1}{2^n} \sum_{a,y,z=0}^{2^n-1} W_a(y) W_a^*(z) e^{2\pi i [y(\phi - m/2^n) - z(\phi - m'/2^n)]} \quad (21b)$$

$$= \frac{1}{2^n} \sum_{y,z=0}^{2^n-1} \delta_{y,z} e^{2\pi i [y(\phi - m/2^n) - z(\phi - m'/2^n)]} \quad (21c)$$

$$= \frac{1}{2^n} \sum_{y=0}^{2^n-1} e^{2\pi i y(m' - m)/2^n} = \delta_{m,m'}, \quad (21d)$$

where Eq. (21c) follows from the unitary condition on the window function preparation $\sum_a W_a(x) W_a^*(x') = \delta_{x,x'}$. \square

Lemma 8. Given $x_i \in \mathbb{R}$ the matrix, X , has only two non-trivial eigenvalues λ_{\pm} :

$$X := \begin{pmatrix} 0 & x_1 & \dots & x_{T-1} \\ x_1 & 0 & \dots & 0 \\ \vdots & \vdots & \ddots & \vdots \\ x_{T-1} & 0 & \dots & 0 \end{pmatrix} \quad \text{and} \quad \lambda_{\pm} = \pm \sqrt{\sum_{i=1}^{T-1} |x_i|^2}.$$

Proof. Consider the characteristic polynomial: $\det(\lambda \mathbb{I} - X) = \lambda^T - \lambda^{T-2} \sum_{i=1}^{T-1} |x_i|^2 = 0$, solving for λ gives,

$$\lambda^T = \lambda^{T-2} \sum_{i=1}^{T-1} |x_i|^2 \quad (22)$$

$$\lambda^2 = \sum_{i=1}^{T-1} |x_i|^2, \quad (23)$$

which has only two solutions stated in the lemma. \square

We finally require the well known result:

Lemma 9. (Spectral stability) Given two Hermitian matrices N and M with ordered eigenvalues $\nu_1 \geq \nu_2 \geq \dots \geq \nu_n$ and $\mu_1 \geq \mu_2 \geq \dots \geq \mu_n$ respectively. For all k

$$\min_j |\nu_j - \mu_k| \leq \|N - M\|_2,$$

where $\|A\|_2 = \sqrt{\lambda_{\max}(A^* A)}$.

See e.g. [43] for a pedagogical proof of Lemma 9. We are now in the position to prove Lemma 3.

Proof. (of Lemma 3) Consider the projectors corresponding to the two described controlled reflections: $P' := \frac{1}{2}(\mathbb{1} - c \cdot R_{\tilde{\psi}_{0,+}})$ and $Q' := \frac{1}{2}(\mathbb{1} - c \cdot \mathcal{B}[\hat{F}])$. Let t be the number of qubits in the system register \mathcal{H}_{sys} . Lemma 1 gives that the eigenspectra of \mathcal{U} can be analysed via the singular values of the projector product. Following the same method as Theorem 2, the corresponding projector product squared is given by,

$$P' \cdot Q' \cdot P' = \sum_{i,j=0}^{2^t-1} \sum_{\pm, \pm'} \alpha_{i,j}^{\pm, \pm'} |\psi_{i, \pm}\rangle \langle \psi_{j, \pm'}|_{\text{sys}, \mathcal{B}_H} \otimes |\rho(\phi_{i, \pm} - \tilde{\phi}_{0,+})\rangle \langle \rho(\phi_{j, \pm'} - \tilde{\phi}_{0,+})|_{\text{iph}} \otimes |0\rangle \langle 0|_{\mathcal{B}_F} \quad (24a)$$

$$= \sum_k |\omega_k|^2 |a_k\rangle \langle a_k|_{\text{sys, iph, } \mathcal{B}_F, \mathcal{B}_H} \quad (24b)$$

where $\alpha_{i,j}^{\pm, \pm'} = \frac{1}{4} \langle \sigma_i | \mathbb{1} - \hat{F} | \sigma_j \rangle \langle \rho(\phi_{i, \pm} - \tilde{\phi}_{0,+}) | 0 \rangle \langle 0 | \rho(\phi_{j, \pm'} - \tilde{\phi}_{0,+}) \rangle$. While Eq. (24a) is not diagonal, it must be brought into the diagonal form in Eq. (24b). It is left to solve for ω_k and $|a_k\rangle$.

If the algorithm is working functionally then $|\langle \rho(\phi_{j \neq 0, \pm} - \tilde{\phi}_{0,+}) | 0 \rangle_{\text{iph}}|$ should be small (corresponding to the reflection not being contaminated too much by excited states). Note also that $\{|\psi_{i, \pm}\rangle \langle \rho(\phi_{i, \pm} - m)\rangle\}_{i, \pm, m}$ is a complete orthogonal basis for $\mathcal{H}_{\text{sys}} \otimes \mathcal{H}_{\text{ph}} \otimes \mathcal{H}_{\mathcal{B}_H}$ (Claim 7). Therefore we look to calculate ω_k relative to the decoupled matrix:

$$\tilde{M} := \sum_{i,j=0}^{2^t-1} \sum_{\pm, \pm'} \beta_{i,j}^{\pm, \pm'} |\psi_{i, \pm}\rangle \langle \psi_{j, \pm'}|_{\text{sys}, \mathcal{B}_H} \otimes |\rho(\phi_{i, \pm} - \tilde{\phi}_{0,+})\rangle \langle \rho(\phi_{j, \pm'} - \tilde{\phi}_{0,+})|_{\text{iph}} \otimes |0\rangle \langle 0|_{\mathcal{B}_F} \quad (25)$$

where

$$\beta_{i,j}^{\pm,\pm'} = \begin{cases} 0 & \text{if } (i=0 \vee j=0) \wedge (\pm = - \vee \pm' = -) \\ \alpha_{i,j}^{\pm,\pm'} & \text{otherwise} \end{cases}$$

Since \tilde{M} is decoupled, it is simple to identify the eigenvector $|\psi_{0,+}\rangle_{\text{sys},\mathcal{B}_H}|\rho(\phi_{0,+} - \tilde{\phi}_{0,+})\rangle_{\text{iph}}|0\rangle_{\mathcal{B}_F}$ with eigenvalue $\frac{1}{4}\langle\sigma_0|\mathbb{1} - \hat{F}|\sigma_0\rangle|\langle\rho(\phi_{0,+} - \tilde{\phi}_{0,+})|0\rangle|^2$.

The difference $\Delta \otimes |0\rangle\langle 0|_{\mathcal{B}_F} := P' \cdot Q' \cdot P' - \tilde{M}$ is a real⁷ symmetric matrix, in the basis $\{|\psi_{i,\pm}\rangle|\rho(\phi_{i,\pm} - m)\rangle\}_{i,\pm,m}$:

$$\Delta = \begin{pmatrix} 0 & F_{0,0}\langle\rho_0^+|0\rangle\langle 0|\rho_0^- \rangle & \dots & F_{0,T-1}\langle\rho_0^+|0\rangle\langle 0|\rho_{T-1}^- \rangle \\ F_{0,0}\langle\rho_0^-|0\rangle\langle 0|\rho_0^+ \rangle & 0 & \dots & 0 \\ F_{1,0}\langle\rho_1^+|0\rangle\langle 0|\rho_0^+ \rangle & \vdots & \ddots & \vdots \\ \vdots & & & \vdots \\ F_{T-1,0}\langle\rho_{T-1}^+|0\rangle\langle 0|\rho_0^+ \rangle & \vdots & & \vdots \\ F_{T-1,0}\langle\rho_{T-1}^-|0\rangle\langle 0|\rho_0^+ \rangle & 0 & \dots & 0 \end{pmatrix}, \quad (26)$$

where for conciseness we introduce the compressed notation $F_{i,j} := \frac{1}{4}\langle\sigma_i|\mathbb{1} - \hat{F}|\sigma_j\rangle$ and $|\rho_i^\pm\rangle := |\rho(\phi_{i,\pm} - \tilde{\phi}_{i,+})\rangle$. Due to the structure of this matrix the only non-zero eigenvalues as per Lemma 8 are given by

$$\pm \sqrt{\left|F_{00}\langle\rho_0^-|0\rangle\langle 0|\rho_0^+ \rangle\right|^2 + \sum_{\sigma \in \pm} \sum_{i=1}^{T-1} \left|F_{0,i}\langle\rho_0^+|0\rangle\langle 0|\rho_i^\sigma \rangle\right|^2}. \quad (27)$$

The maximum difference between an eigenvalue of \tilde{M} and the closest eigenvalue of $P' \cdot Q' \cdot P'$ is upper bounded by the operator norm of the difference (Lemma 9) therefore,

$$\min_j \left| \lambda_j(P' \cdot Q' \cdot P') - F_{00} \left| \langle\rho_0^+|0\rangle \right|^2 \right| \leq \|\Delta\|_{\text{op}} \quad (28a)$$

$$= \sqrt{\left|F_{00}\langle\rho_0^-|0\rangle\langle 0|\rho_0^+ \rangle\right|^2 + \sum_{\pm} \sum_{i=1}^{T-1} \left|F_{0,i}\langle\rho_0^+|0\rangle\langle 0|\rho_i^\pm \rangle\right|^2} \quad (28b)$$

$$\leq 2 \left| \langle\rho_0^+|0\rangle \right| \max_{j>0 \in [0,2^{t-1}], \pm} \left\{ \left| \langle 0|\rho_j^\pm \rangle \right|, \left| \langle 0|\rho_0^- \rangle \right| \right\} \sum_{i=0}^{2^t-1} |F_{0,i}| \quad (28c)$$

$$\leq 2 \left| \langle\rho_0^+|0\rangle \right| \max_{j>0 \in [0,2^{t-1}], \pm} \left\{ \left| \langle 0|\rho_j^\pm \rangle \right|, \left| \langle 0|\rho_0^- \rangle \right| \right\} \quad (28d)$$

The final line follows since $\sum_{i=0}^{2^t-1} |F_{0,i}| \leq \max_k \sum_{i=0}^{2^t-1} |F_{k,i}|$ is upper bounded by the infinity matrix norm which is sub-multiplicative. Since \hat{F} is a bounded Hermitian matrix there exists a unitary U such that $\hat{F} = U^\dagger D U$ where D is a diagonal bounded matrix. Therefore $\|\hat{F}\|_{\text{op}} \leq \|U^\dagger\|_{\text{op}} \|D\|_{\text{op}} \|U\|_{\text{op}} \leq 1$, where $\|D\|_{\text{op}} \leq 1$ and $\|U\|_{\text{op}} = 1$.

Returning to the result statement, Lemma 1 gives that the unitary \mathcal{U} has eigenphases $\theta_{0,\pm} = \pm \frac{1}{2\pi} \cos^{-1} (2|\omega|^2 - 1)$. The singular values ω correspond to the absolute squared values of the eigenvalues of the projector product $\lambda(P' \cdot Q' \cdot P') = |\omega|^2$. Hence, Eq. (28d) leads directly to the result

⁷Real due to the phase factors absorbed to the basis.

statement:

$$|\omega|^2 = F_{00} |\langle \rho_0^+ | 0 \rangle|^2 \pm 2 \left| \langle \rho_0^+ | 0 \rangle \right| \max_{j > 0 \in [0, 2^t - 1], \pm} \left\{ \left| \langle 0 | \rho_j^\pm \rangle \right|, \left| \langle 0 | \rho_0^- \rangle \right| \right\} \quad (29a)$$

$$= \frac{1}{4} \langle \sigma_0 | \mathbb{1} - \hat{F} | \sigma_0 \rangle |\langle \rho_0^+ | 0 \rangle|^2 \pm 2 \left| \langle \rho_0^+ | 0 \rangle \right| \max_{j > 0 \in [0, 2^t - 1], \pm} \left\{ \left| \langle 0 | \rho_j^\pm \rangle \right|, \left| \langle 0 | \rho_0^- \rangle \right| \right\}. \quad (29b)$$

□

A.4 Proof of error analysis

Proposition 5. (Expectation value algorithm error analysis) *A successful instance of Algorithm 1 outputs an ϵ -approximation of $\langle \sigma_0 | \hat{F} | \sigma_0 \rangle$ where*

$$\epsilon \leq \frac{3\pi 2^{-n_o} + 8 |\langle \rho_0^+ | 0 \rangle| \max_{j > 0, \pm} \left\{ |\langle 0 | \rho_j^\pm \rangle|, |\langle 0 | \rho_0^- \rangle| \right\} + c}{|\langle \rho_0^+ | 0 \rangle|^2},$$

given $|\rho_j^\pm\rangle_{\text{iph}} := \frac{1}{\sqrt{2^n}} \sum_{a,x=0}^{2^n-1} W_a^*(x) e^{-2\pi i (\phi_{j,\pm} - \tilde{\phi}_{0,+})x} |a\rangle_{\text{iph}}$, the number of qubits in the phase register of the oQPE is n_o and c is a free non-negative constant.

Proof. Recapping the three contributions of error:

1. **Reflection error** $\epsilon_1 := |\omega|^2 - f(\langle \sigma_0 | \hat{F} | \sigma_0 \rangle)$, due to the eigenvalue of the projector product deviating from the decoupled matrix, where $f(X) = \frac{|\langle \rho_0^+ | 0 \rangle|^2}{4}(1 - X)$. From Lemma 3, $\epsilon_1 \leq |\langle \rho_0^+ | 0 \rangle| 2 \max_{j > 0, \pm} \left\{ |\langle 0 | \rho_j^\pm \rangle|, |\langle 0 | \rho_0^- \rangle| \right\}$.
2. **Pre-learning error**, of the estimate $|\langle \rho_0^+ | 0 \rangle|^2 \pm \delta(|\langle \rho_0^+ | 0 \rangle|^2)$. Recall that for the first step of the algorithm is to run the circuit with the identity observable to obtain as estimate of this value that will be used to compute the final expectation value from the obtained measurement. The error in this estimate is dominated by the bit discretisation of the oQPE. The oQPE estimates $\theta'_\pm = \pm \frac{1}{\pi} \cos^{-1}(2|\langle \rho_0^+ | 0 \rangle|^2 - 1)$, bit discretisation gives $\delta(\theta') = 2^{-n_o}$ therefore $\delta(|\langle \rho_0^+ | 0 \rangle|^2) = \pi \sqrt{|\langle \rho_0^+ | 0 \rangle|^2 (1 - |\langle \rho_0^+ | 0 \rangle|^2)} \delta(\theta') \leq \pi 2^{-(n_o+1)}$.
3. **oQPE error** from imperfect estimation of the iterate eigenphase due to bit discretisation in the outer QPE, $|\theta_{0,\pm} - \tilde{\theta}_{0,\pm}| \leq 2^{-(n_o+1)}$.

Lemma 1 shows that the eigenphase of the iterate \mathcal{U} is related to the squared eigenvalues of the projector product by, $\theta_\pm = \pm \frac{1}{2\pi} \cos^{-1}(2\omega^2 - 1)$. Propagation of errors gives $\frac{d\theta}{d(\omega^2)} = -\frac{1}{2\pi\sqrt{\omega^2(1-\omega^2)}}$ we can relate error in θ to error in the squared eigenvalue,

$$\delta(\omega^2) = \frac{d(\omega^2)}{d\theta} \delta\theta = 2\pi\sqrt{\omega^2(1-\omega^2)} \delta\theta, \quad (30)$$

where $\delta(\cdot)$ denotes the absolute error. Therefore, $\delta(f(\langle \sigma_0 | \hat{F} | \sigma_0 \rangle)) = \delta(|\omega|^2) + \epsilon_1$. Relate this to the error in $\langle \sigma_0 | \hat{F} | \sigma_0 \rangle$, by introducing the notation $\langle F \rangle := \langle \sigma_0 | \hat{F} | \sigma_0 \rangle$, $p = |\langle \rho_0^+ | 0 \rangle|^2$ and defining

$$g(X) := \frac{f(X)}{p} = \frac{1}{4}(1 - X):$$

$$\left(\frac{\delta(g(\langle F \rangle))}{g(\langle F \rangle)} \right)^2 = \left(\frac{\delta(f(\langle F \rangle))}{f(\langle F \rangle)} \right)^2 + \left(\frac{\delta(p)}{p} \right)^2 \quad (31a)$$

$$\delta(g(\langle F \rangle))^2 = \frac{\delta(f(\langle F \rangle))^2}{p^2} + \frac{g(\langle F \rangle)^2 \delta(p)^2}{p^2} \quad (31b)$$

$$\delta(g(\langle F \rangle))^2 \leq \frac{\delta(f(\langle F \rangle))^2}{p^2} + \frac{\delta(p)^2}{4p^2} \quad (31c)$$

$$\delta(g(\langle F \rangle)) \leq \frac{1}{p} \sqrt{\delta(f(\langle F \rangle))^2 + \delta(p)^2/4}. \quad (31d)$$

Since $\langle F \rangle \in [-1, 1]$ we can upper bound $g(\langle F \rangle) \leq \frac{1}{2}$. Then we have,

$$\delta(\langle F \rangle) = 4\delta(g(\langle F \rangle)) \quad (32a)$$

$$\leq \frac{4}{p} \sqrt{\delta(f(\langle F \rangle))^2 + \delta(p)^2/4}. \quad (32b)$$

Combining all these components we have,

$$\left| \langle \sigma_0 | \hat{F} | \sigma_0 \rangle - F_{\text{est}} \right| = \delta(\langle F \rangle) \quad (33a)$$

$$\leq \frac{4}{p} \sqrt{\delta(f(\langle F \rangle))^2 + \delta(p)^2/4} \quad (33b)$$

$$\leq \frac{4}{p} \sqrt{[\delta(|\omega|^2) + \epsilon_1]^2 + \left[\frac{\pi 2^{-n_o}}{2} \right]^2} \quad (33c)$$

$$\leq \frac{4[\delta(|\omega|^2) + \epsilon_1]}{p} + \frac{\pi 2^{-n_o}}{p} \quad (33d)$$

$$\leq \frac{4}{p} \left[2\pi 2^{-(n_o+1)} \sqrt{\omega^2(1-\omega^2)} + \epsilon_1 \right] + \frac{\pi 2^{-n_o}}{p} \quad (33e)$$

$$\leq \frac{3\pi 2^{-n_o}}{p} + \frac{4\epsilon_1}{p}. \quad (33f)$$

Finally substituting in for ϵ_1 and $p := |\langle \rho_0^+ | 0 \rangle|^2$ gives,

$$\epsilon \leq \frac{3\pi 2^{-n_o} + 8|\langle \rho_0^+ | 0 \rangle| \max_{j>0,\pm} \{ |\langle 0 | \rho_j^\pm \rangle|, |\langle 0 | \rho_0^- \rangle| \} + c}{|\langle \rho_0^+ | 0 \rangle|^2}, \quad (34)$$

where c is any non-negative constant. Since this loosens the bound we are free to set this constant. \square

A.5 Proof of success probability

To prove the success probability we use the following well known result about perturbation of eigenvectors.

Theorem 10. (Davis-Kahan [38]) *Let $A, B \in \mathbb{C}^{T \times T}$ be Hermitian. For $i \in \{1, \dots, T\}$ given that*

$$\delta := \min_{j \neq i} |\lambda_i(A) - \lambda_j(A)| > 0,$$

then

$$\min_{s \in \{\pm 1\}} \|v_i(A) - sv_i(B)\|^2 \leq \frac{8\|A - B\|_2^2}{\delta}.$$

For a proof of Theorem 10 see [38].

Proposition 6. (Expectation value algorithm success probability) *Algorithm 1 succeeds with probability,*

$$p_{\text{success}} \geq |\langle 0 | \rho_0^+ \rangle|^2 \left(1 - \frac{32 \max_{j>0,\pm} \{ |\langle 0 | \rho_j^\pm \rangle|, |\langle 0 | \rho_0^- \rangle| \}^2}{c} \right),$$

where $|\rho_j^\pm\rangle_{\text{iph}} := \frac{1}{\sqrt{2^n}} \sum_{a,x=0}^{2^n-1} W_a^*(x) e^{-2\pi i (\phi_{j,\pm} - \tilde{\phi}_{0,+})x} |a\rangle_{\text{iph}}$ and c is the free non-negative constant from the error tolerance.

Proof. In correspondence with Proposition 5 the probability of success is defined as obtaining an estimate to the expectation value that is accurate to within the error tolerance given in the error bound. Practically this amounts to a success probability defined as $p_{\text{success}} := |\langle \psi_{0,+} | \langle \rho_0^+ | \langle 0 | \sum_{k \in \mathcal{K}} |a_k\rangle |^2$ where $\{|a_k\rangle\}_{k \in \mathcal{K}}$ is the set of eigenvectors of the projector product of the iterate \mathcal{U} with eigenvalues $|\lambda_k - F_{00}| \langle \rho_0^+ | 0 \rangle|^2 < 2 \max_{j>0,\pm} \{ |\langle 0 | \rho_j^\pm \rangle|, |\langle 0 | \rho_0^- \rangle| \}$.

As in Lemma 1 we express the eigenvectors of $P' \cdot Q' \cdot P'$ as a perturbation from those of the decoupled matrix \tilde{M} .

$$P' \cdot Q' \cdot P' = \sum_{i,j=0}^{2^t-1} \sum_{\pm,\pm'} \alpha_{i,j}^{\pm,\pm'} |\psi_{i,\pm}\rangle \langle \psi_{j,\pm'}|_{\text{sys},\mathcal{B}_H} \otimes |\rho(\phi_{i,\pm} - \tilde{\phi}_{0,+})\rangle \langle \rho(\phi_{j,\pm'} - \tilde{\phi}_{0,+})|_{\text{iph}} \otimes |0\rangle \langle 0|_{\mathcal{B}_F} \quad (35)$$

where $\alpha_{i,j}^{\pm,\pm'} = \frac{1}{4} \langle \sigma_i | \mathbb{1} - \hat{F} | \sigma_j \rangle \langle \rho(\phi_{i,\pm} - \tilde{\phi}_{0,+}) | 0 \rangle \langle 0 | \rho(\phi_{j,\pm'} - \tilde{\phi}_{0,+}) \rangle$ and

$$\tilde{M} := \sum_{i,j=0}^{2^t-1} \sum_{\pm,\pm'} \beta_{i,j}^{\pm,\pm'} |\psi_{i,\pm}\rangle \langle \psi_{j,\pm'}|_{\text{sys},\mathcal{B}_H} \otimes |\rho(\phi_{i,\pm} - \tilde{\phi}_{0,+})\rangle \langle \rho(\phi_{j,\pm'} - \tilde{\phi}_{0,+})|_{\text{iph}} \otimes |0\rangle \langle 0|_{\mathcal{B}_F} \quad (36)$$

where

$$\beta_{i,j}^{\pm,\pm'} = \begin{cases} 0 & \text{if } (i=0 \vee j=0) \wedge (\pm = - \vee \pm' = -) \\ \alpha_{i,j}^{\pm,\pm'} & \text{otherwise.} \end{cases}$$

To prove statements about the perturbation of eigenvectors requires knowledge of the eigengap of the matrix, δ as described in Theorem 10. Substitute $\tilde{M} = A$ and $P' \cdot Q' \cdot P' = B$ into Theorem 10 and look at i such that $v_i(\tilde{M}) = |\psi_{0,+}\rangle \langle \rho_0^+ | 0 \rangle$ and $\lambda_i(\tilde{M}) = F_{00} |\langle \rho_0^+ | 0 \rangle|^2$ (recall the compressed notation: $F_{i,j} := \frac{1}{4} \langle \sigma_i | \mathbb{1} - \hat{F} | \sigma_j \rangle$ and $|\rho_i^\pm\rangle := |\rho(\phi_{i,\pm} - \tilde{\phi}_{0,+})\rangle$). Using the bound on the operator norm of $\Delta \otimes |0\rangle \langle 0|_{\mathcal{B}_F} := P' \cdot Q' \cdot P' - \tilde{M}$ from Lemma 3:

$$\min_{s \in \{\pm 1\}} \left\| |\psi_{0,+}\rangle \langle \rho_0^+ | 0 \rangle - s v_i(P' \cdot Q' \cdot P') \right\|^2 \leq \frac{8 \|\Delta\|_{\text{op}}^2}{\delta} \quad (37a)$$

$$\leq \frac{32 |\langle \rho_0^+ | 0 \rangle|^2 \max_{j>0,\pm} \{ |\langle 0 | \rho_j^\pm \rangle|, |\langle 0 | \rho_0^- \rangle| \}^2}{\delta}. \quad (37b)$$

The eigengap δ is the gap between the eigenvalue $\lambda_i(\tilde{M}) = F_{00} |\langle \rho_0^+ | 0 \rangle|^2$ and the next closest eigenvalue of \tilde{M} . Due to the decoupled nature of \tilde{M} the other eigenvalues correspond to a sub-matrix without support on the $v_i(\tilde{M}) = |\psi_{0,+}\rangle \langle \rho_0^+ | 0 \rangle$ basis. Recycling the argument from Lemma 3 we know that the operator norm of this sub-matrix is small.

We then separate into two cases and analyse these separately,

Case 1: $\lambda_i(\tilde{M}) = F_{00}|\langle\rho_0^+|0\rangle|^2$ is the largest eigenvalue of \tilde{M} and is lower bounded by

$$\lambda_i(\tilde{M}) \geq 2|\langle\rho_0^+|0\rangle| \max_{j>0,j\pm} \left\{ |\langle 0|\rho_j^\pm\rangle|, |\langle 0|\rho_0^-\rangle| \right\} + c$$

Case 2: Otherwise $\lambda_i(\tilde{M})$ is itself small: $\lambda_i(\tilde{M}) < 2|\langle\rho_0^+|0\rangle| \max_{j>0,j\pm} \left\{ |\langle 0|\rho_j^\pm\rangle|, |\langle 0|\rho_0^-\rangle| \right\} + c$

for some non-zero constant c . These two cases clearly encapsulate all possible scenarios for any value of c , in practice we set c bounded away from 0 so that if the eigengap is closing we do not use Theorem 10 to bound the success probability and instead consider that all eigenvectors lie within the error tolerance.

Case 1 analysis: λ_i is large so that the closest eigenvalue to λ_i is now the maximum eigenvalue of the sub-matrix. Since $|F_{i,j}| \leq 1/2$ we can upper bound the maximum eigenvalue of the sub-matrix by $2|\langle\rho_0^+|0\rangle| \max_{j>0,\pm} \left\{ |\langle 0|\rho_j^\pm\rangle|, |\langle 0|\rho_0^-\rangle| \right\}$. Hence the eigengap is lower bounded by $\delta \geq c$ – note that here if we consider c going to zero the success probability from Theorem 10 vanishes. Substituting this into Eq. (37b) gives

$$\min_{s \in \{\pm 1\}} \left\| |\psi_{0,+}\rangle|\rho_0^+\rangle|0\rangle - sv_i(P' \cdot Q' \cdot P') \right\|^2 \leq \frac{32|\langle\rho_0^+|0\rangle|^2 \max_{j>0,\pm} \left\{ |\langle 0|\rho_j^\pm\rangle|, |\langle 0|\rho_0^-\rangle| \right\}^2}{c} \quad (38)$$

The probability of success is then given by $p_{\text{success}} \geq |\langle 0|\rho_0^+\rangle|^2 \left(1 - \frac{32 \max_{j>0,\pm} \left\{ |\langle 0|\rho_j^\pm\rangle|, |\langle 0|\rho_0^-\rangle| \right\}^2}{c} \right)$ since the state prepared is $|\psi_{0,+}\rangle_{\text{sys},\mathcal{B}_H}|0\rangle_{\text{iph}}|0\rangle_{\mathcal{B}_F}$.

Case 2 analysis: Here the eigenvalue of interest, λ_i , is itself small, and hence the eigengap closes as c decreases, allowing the eigenvectors to mix and the overlap between the initial state and the eigenvector corresponding to λ_i will decrease. However, this can only happen since all the eigenvalues are now close, so while the algorithm may estimate an eigenvalue corresponding to a different eigenvector this is an $(2|\langle\rho_0^+|0\rangle| \max_{j>0,\pm} \{ |\langle 0|\rho_j^\pm\rangle|, |\langle 0|\rho_0^-\rangle| \} + c)$ -approximation of the desired eigenvalue with probability 1. For consistency this does however increase the error for the estimate which is why $4c/p$ appears as an additional error in Proposition 5.

Since all outcomes in case 2 results in an estimate of the expectation value within the error tolerance of Proposition 5 the total success probability is given by the expression for case 1. The additional error in the eigenvalue c must be taken to be a non-negative value and coincides with the extra tolerance added to the error bound in Proposition 5. \square

B Resource estimation details

This appendix details how the numerics quoted in Fig. 5 and Table 1 were generated. We first give an overview, and then give specifics on the use of BLISS-THC and the error model used to do the truncation as well as the corresponding data.

B.1 Overview

Overall Toffoli cost: Fig. 5 gives a quantum resource estimates for the number of Toffoli gates required to learn a physical observable (kinetic energy, x -dipole moment and ERI) with respect to different molecular systems. Recall some notation from the algorithm: the arbitrary state preparation unitary for the initial state of the system ASP; the unitary that prepares the window state \hat{W} ; the qubitised encoding of the Hamiltonian $\mathcal{Q}[H]$; a quantum Fourier transform on x qubits QFT_x ; the self-inverse encoding of the observable $\mathcal{B}[F]$; the number of phase qubits in the outer QPE n_0 and the number of phase qubits in the inner QPE n . From examining the circuit diagram in Fig. 2a, assuming a simple additive gate count model, the approximate cost of one run of the full algorithm is given by:

$$\mathcal{T}(\text{ASP}) + 2^{n_0} \mathcal{T}(\hat{W}) + 2^{n_0+n-1} \mathcal{T}(\mathcal{Q}[H]) + 2^{n_0+1} \mathcal{T}(\text{QFT}_n) + 2^{n_0-1} \mathcal{T}(\mathcal{B}[F]) + \mathcal{T}(\text{QFT}_{n_0}), \quad (39)$$

where $\mathcal{T}(\cdot)$ denotes the Toffoli cost associated with that operation.

In textbook QPE a phase register of n' qubits requires $\sum_{r=0}^{n'-1} 2^r = 2^{n'} - 1$ calls the controlled unitary, one call to a phase state preparation unitary and one to a $\text{QFT}_{n'}$. However, by controlling on both subspaces of each phase register qubit and applying both U and U^\dagger (see for example [3][Figure 2]) the number of unitary calls can be squeezed by roughly⁸ a factor of 2. Therefore, given n_0 outer phase qubits, $\mathcal{T}(\text{oQPE}) = 2^{n_0-1} \mathcal{T}(\mathcal{U}) + \mathcal{T}(\text{QFT}_{n_0})$. The walk operator can be further decomposed as $\mathcal{T}(\mathcal{U}) = 2\mathcal{T}(\text{iQPE}) + \mathcal{T}(\text{Refl}_{\text{iph}}) + \mathcal{T}(\text{c-B}[F])$. Finally the inner QPE with n total phase qubits requires $\mathcal{T}(\text{iQPE}) = 2^{n-1} \mathcal{T}(\mathcal{Q}[H]) + \mathcal{T}(\text{QFT}_n) + \mathcal{T}(\hat{W})$. Putting this together yields the expression for the total cost in Eq. (39).

This expression highlights that the leading cost in the algorithm is the block encoding of the Hamiltonian due to the large number of repetitions required. We find that the Toffoli cost of the other components is negligible compared to the block encodings, therefore only the cost of the Hamiltonian and observable encodings where included in Fig. 5.

Overall logical qubit cost: The logical qubit estimates given in Table 1 correspond to the qubit highwater – the maximum number of logical qubits required to be in coherent superposition at any given point in the circuit. Subroutines will require temporary ancillae that are released at the end of the routine by uncomputes. This is opposed to persistent ancillae, which cannot be reused freely, as they are either referenced by gates in later subroutines or remain entangled. Not reusing the temporary ancillae across subroutines can greatly overestimate the resources required to run the algorithm and so this distinction between temporary and persistent is essential. Not accounting for reusing the temporary ancilla across routines makes for the significantly higher logical qubit counts reported in previous estimates [40]. In addition to the temporary ancillae the logical qubit count includes all registers that are pervasive through the algorithm (those that appear explicitly in Fig. 2a). Qubit highwater additions due to state preparation and QSP implementation are neglected.

Error budgeting: As part of the problem instance we set an absolute error tolerance ϵ_{target} for the expectation value. These are chosen to be reasonable with respect to literature: $\epsilon_{\text{kin.}} = 1.6 \text{ mHa}$, $\epsilon_{\text{dip.}} = 10 \text{ mDebye}$, and $\epsilon_{\text{eri}} = 1.6 \text{ mHa}$. For the numerics we assume perfect gate implementation and state preparation, however due to the limited qubit registers the algorithm will only estimate

⁸ Additionally if the unitary is comprised of a product of reflections – as is the case for both QPE subroutines in this algorithm – further reductions can be made by not controlling some of the reflections.

the expectation value approximately, as discussed at length in Appendix A.4. The error, ϵ_{inner} is the contribution to the final estimate from the inner QPE ($\epsilon_{\text{inner}} = \frac{4\epsilon_1}{p}$ from Eq. (33f)) and $\epsilon_{\text{inner}}/\lambda_F$ is plotted in Fig. 4 for various window functions. The outer error, ϵ_{outer} , is the contribution to the final estimate from the inner QPE ($\epsilon_{\text{outer}} = \frac{3\pi 2^{-n_o}}{p}$ from Eq. (33f)) and is exponentially suppressed by increasing the size of the outer phase register.

Furthermore, the dominant contribution to the resource estimation is the cost of the block encoding. The block encoding implementation introduces another error from data truncation. To obtain numerical estimates, this error must be budgeted for and so we introduce ϵ_{data} as the absolute error contribution due to the chosen implementation of the block encoding. Hence, we require a total error target decomposition,

$$\epsilon_{\text{target}} = \epsilon_{\text{inner}} + \epsilon_{\text{outer}} + \epsilon_{\text{data}}. \quad (40)$$

For the numerics quoted in Fig. 4, a simple error distribution of $\epsilon_{\text{inner}} = \epsilon_{\text{outer}} = \epsilon_{\text{data}} = \epsilon_{\text{target}}/3$ was chosen. Some preliminary optimisation was done between ϵ_{inner} and ϵ_{outer} and it was found that although it varied between instance, and equal split was close to optimal. We leave further optimisation through refinement of the error model to future work.

Number of inner phase qubits, $n = l + m$: The “baseline” inner QPE number of qubits l is chosen such that the ground state of the Hamiltonian can be distinguished from the first excited state. This requires an estimate for the Hamiltonian one-norm λ_H and an upper bound on the spectral gap Δ . The relationship between the number of qubits required to distinguish the ground state of the qubitised Hamiltonian is given by

$$l = \left\lceil \log_2 \left(\frac{2\pi\lambda_H}{\Delta} \right) \right\rceil. \quad (41)$$

Recalling the relation between the eigenphase of a qubitised operator and its spectra we require

$$\frac{1}{2\pi} \left| \cos^{-1} \left(\frac{\lambda_0}{\lambda_H} \right) - \cos^{-1} \left(\frac{\lambda_0 + \Delta}{\lambda_H} \right) \right| > \frac{1}{2^l},$$

where λ_0 is the ground state energy of the system. The left-hand side is minimised by $\lambda_0 = 0$, we then expand $\cos^{-1}(x) \approx \frac{\pi}{2} - x$ assuming the relative spectral gap is small.

In both the standard rectangular QPE and the Kaiser-windowed version the success amplitude is improved by adding additional phase qubits m – see Fig. 4. The minimum number of additional qubits m is chosen such that the relative error budget $\epsilon_{\text{inner}}/\lambda_F$, is below the threshold.

Number of outer phase qubits n_o : The number of outer QPE phase qubits is given by

$$n_o = \left\lceil \log_2 \left(\frac{3\pi\lambda_F}{p\epsilon_{\text{outer}}} \right) \right\rceil, \quad (42)$$

where we recall that $p = |\langle \rho_0^+ | 0 \rangle|^2$. For the rectangular window this is lower bounded by $4/\pi^2$ whereas for the Kaiser window this is calculated from Fig. 3 [Right] for the chosen β . Recall that the phase estimated by the outer QPE corresponds to $\theta = \pm \frac{1}{2\pi} \cos^{-1}(2|\omega|^2 - 1)$ where $|\omega|^2 = \frac{p}{4}(1 - \langle F \rangle)$. The relationship between the phase error and the expectation value error is governed by Proposition 5. The error induced by a finite outer phase register is 2^{-n_o} , which leads to the expression in Eq. (42).

Estimating problem parameters: To obtain representative resource estimates for the expectation value algorithm we quote three different observables over four different systems of varying complexity. The one-norm and spectral gap of each system Hamiltonian, in addition to the one-norm of all observables, must be estimated to inform the algorithmic requirements such as the number of phase qubits. We follow [40] in defining the three closed-shell systems – refer to [40, Table V] for details of the molecular geometries used for the calculations, where the cc-pVDZ basis set is used throughout

all computations. For the heme (P450) system, we use the active space selected in [11], and refer to [11, Appendix I] for details on the system parameters. The spectral gap is computed with DMRG at bond dimension $M = 1000$; applied to the full all-electron space for ammonia and water, and to a (30e, 30o) active space for p-Benzene. We refer readers to [40] and [11] for further details on these calculations. The values used for the resource estimate are quoted in Table 2.

System	Property	
	N	Δ
Water	24	0.302
Ammonia	29	0.280
P450 heme	43	0.0069
p-Benzene	104	0.114

Table 2: Hamiltonian spectral gap estimate, Δ_H , in Hartree used in the quantum resource estimate. We follow [40] in defining the systems for a fair comparison.

Block encoding of the Hamiltonian and observable: Both the observable and system Hamiltonian are block encoded following the optimised tensor hypercontraction implementation [8]. Compared to a previous work [25], this implementation provided further reductions based on using fused adders for Givens orbital rotation gates, improved bit precision allocation for rotation angles, as well as other minor improvements. We refer readers to [8] for exact details on the block-encoding implementation. Furthermore, a single error budget, ϵ_{data} , is used for all of the block-encoding data loading, which is estimated classically. This procedure is described in more detail in Appendix B.2 where the ranks and bit precisions used to generate the data in Section 3 are quoted.

Subleading costs: The block encoding repetitions constitute the major cost and we find the ASP, QFTs and window preparation unitary contributions are negligible in comparison. The benefits of using a tapered phase state in the quantum phase estimation, comes at the cost of having to prepare a more complicated state than uniform superposition. The parameters that effect the efficiency of preparing the Kaiser window are: number of qubits n , bandwidth β and error η . When assessing state preparation routines for a function $\sum_x |g(x)\rangle$, there are two broad camps we consider: methods that require an amplitude oracle $\sum_x |x\rangle |0\rangle \mapsto \sum_x |x\rangle |\tilde{g}(x)\rangle$ [17, 28] and those that do not [30]. While both require significant classical pre-processing – the former in classical computation of the amplitudes and the latter in computation of high-order Taylor series – we will neglect this and focus on the quantum resources. The main advantage of not using an amplitude oracle is the lower ancilla cost. The Hamiltonian block encoding required for the QPE uses many ancillae and therefore using a qubit-expensive but gate efficient state preparation does not impact the qubit highwater. To investigate the subleading nature simple Grover-Rudolph type state preparation was investigated⁹.

B.2 Block encoding error handling for expectation value estimation

The two-body observables and Hamiltonians are represented with BLISS-THC, therefore we need a rank and finite bit precision approximation for both operators. The minimum rank and bit precision parameters are chosen such that

$$\left| \langle \sigma_0(\hat{H}) | \hat{F} | \sigma_0(\hat{H}) \rangle_{\text{corr}} - \langle \sigma_0(\tilde{H}) | \tilde{F} | \sigma_0(\tilde{H}) \rangle_{\text{corr}} \right| < \epsilon_{\text{data}} \quad (43)$$

⁹There is scope to optimise this sub-routine using a space-time trade off due to the ancillae needed for the block encoding, but as it is already a subleading contribution other optimisation should be prioritised.

where \hat{F}/\hat{H} are the unnormalised target observable/Hamiltonian operators without truncation and \tilde{F}/\tilde{H} are the unnormalised observable/Hamiltonian operators truncated to the rank and bit precision parameters used in each block-encoding scheme¹⁰. Similar to previous works [25, 8], we choose the minimum rank and bit precision parameters based on the expectation value of the correlation component of the 1- and 2-body Reduced Density Matrices (1- and 2-RDMs). In other words, it is assumed that the full expectation value can be decomposed as, $\langle \sigma_0(\hat{H})|\hat{F}|\sigma_0(\hat{H}) \rangle = \langle \sigma_0(\hat{H})|\hat{F}|\sigma_0(\hat{H}) \rangle_{\text{HF}} + \langle \sigma_0(\hat{H})|\hat{F}|\sigma_0(\hat{H}) \rangle_{\text{corr}}$, where the first term uses the Hartree-Fock 1- and 2-RDMs, while the second term uses the remaining traceless correlation-component 1- and 2-RDMs. This implies that the actual observable estimate used in the expectation value algorithm will be, $\langle \hat{F} \rangle_{\text{est.}} = \langle \sigma_0(\hat{H})|\hat{F}|\sigma_0(\hat{H}) \rangle_{\text{HF}} + \langle \sigma_0(\hat{H})|\tilde{F}|\sigma_0(\hat{H}) \rangle_{\text{corr}}$, where the approximate Hartree-Fock contribution is subtracted out and replaced with a Hartree-Fock observable estimate based on non-truncated Hamiltonian and observables. We find that this methodology improves the overall truncation scheme with errors that converge more reliably.

Since FCI-level calculations are not possible beyond small system sizes, we estimate $\langle \sigma_0(\hat{H})|\hat{F}|\sigma_0(\hat{H}) \rangle$ using coupled cluster singles and doubles (CCSD), which provide 1- and 2-RDMs necessary for observable estimation. The truncated expectation value, $\langle \sigma_0(\hat{H})|\tilde{F}|\sigma_0(\hat{H}) \rangle$, is also estimated with same CCSD procedure performed with the truncated Hamiltonian and associated observable. In all cases, we are able to achieve $\epsilon_{\text{data}} = \epsilon_{\text{target}}/3$ with the ranks, norms and bit precision parameters given in Tables 3 to 5.

System	λ_H (E _h)	M_H	\aleph_H, \beth_H	λ_K (E _h)	\aleph_K, \beth_K	CCSD corr. error (mE _h)
Water	107.49	80	13	69.16	9	0.445
Ammonia	128.91	80	14	57.25	11	0.427
P450 heme	87.34	160	19	58.66	13	0.437
p-Benzene	660.91	440	16	199.25	13	-0.398

Table 3: Block encoding details of the *kinetic energy operator* and the Hamiltonian used in for the quantum resource estimate in Fig. 5. Since kinetic energy is a one body operator, BLISS-THC is not required. The one-body operator is block-encoded via an eigendecomposition, followed by symmetry-shifting of the eigenvalues to reduce the one-norm. For each system the following properties are given: λ_H (λ_K) the one-norm of the Hamiltonian (kinetic energy operator) in Hartree; M_H the THC rank of the Hamiltonian; \aleph_H (\aleph_K) the number of bits of precision used for the ‘keep’ probabilities in alias sampling within the Hamiltonian (kinetic energy operator) block encoding; \beth_H (\beth_K) the number of bits of precision in the Givens rotation angles required for the SELECT operator of the Hamiltonian (kinetic energy operator); observable correlation error based on coupled cluster singles and doubles (CCSD) reduced density matrices, following the procedure discussed after Eq. (43). For all the observables considered here we take $\aleph_H = \beth_H$ and $\aleph_K = \beth_K$ to simplify the optimisation.

¹⁰Note that elsewhere we use F, H with $\|F\|_{\text{op}}, \|H\|_{\text{op}} \leq 1$, but for this classical prepossessing step we refer to the unnormalised operators.

System	λ_H (E _h)	M_H	\aleph_H, \beth_H	λ_D (a.u.)	\aleph_D, \beth_D	CCSD corr. error ($\times 10^{-3}$ a.u.)
Water	105.66	60	10	20.70	10	-0.630
Ammonia	118.66	80	10	28.39	10	0.608
P450 heme	84.04	140	15	38.43	14	-0.550
p-Benzene	660.22	430	17	238.59	13	-0.950

Table 4: Block encoding details of the *dipole observable* in the x direction and the Hamiltonian used in for the quantum resource estimate in Fig. 5. Since the dipole moment operator is a one-body operator, BLISS-THC is not required. The one-body operator is block-encoded via an eigendecomposition, followed by symmetry-shifting of the eigenvalues to reduce the 1-norm. See Table 3 for a description of the table headings. λ_D is the one norm of the dipole operator in atomic units.

System	λ_H (E _h)	M_H	\aleph_H, \beth_H	λ_I (E _h)	M_I	\aleph_I, \beth_I	CCSD corr. error (mE _h)
Water	103.83	70	13	114.84	60	12	0.406
Ammonia	139.40	80	11	120.95	90	10	-0.042
P450 heme	85.60	150	13	133.94	140	13	-0.021
p-Benzene	727.33	430	13	621.68	430	15	-0.370

Table 5: Block encoding details of the *electron repulsion integral (ERI)* and the Hamiltonian used in for the quantum resource estimate in Fig. 5. This is an example of a two-body operator and so here both the Hamiltonian and observable are block encoded using the BLISS-THC technique. See Table 3 for a description of the table headings. λ_I is the one norm of the ERI in Hartree.